The Astronomical Journal, 134:1827–1842, 2007 November

CO(1–0), CO(2–1), AND NEUTRAL GAS IN NGC 6946: MOLECULAR GAS IN A LATE-TYPE, GAS-RICH, SPIRAL GALAXY

Lucian P. Crosthwaite
Unmanned Systems, Northrop Grumman, San Diego, CA 92150, USA; lpcrosthwaite@cox.net

and

Jean L. Turner
Division of Astronomy and Astrophysics, UCLA, Los Angeles, CA 90095, USA; turner@astro.ucla.edu
Received 2005 July 2; accepted 2007 July 15

ABSTRACT

We present on-the-fly maps of the CO(1–0) and CO(2–1) emission covering a $10' \times 10'$ region of NGC 6946. Using our CO maps and archival VLA H I observations we create a total gas surface density map, $\Sigma_{\rm gas}$, for NGC 6946. The predominantly molecular inner gas disk transitions smoothly into an atomic outer gas disk, with equivalent atomic and molecular gas surface densities at $R = 3.5'$ (6 kpc). We estimate that the total H_2 mass is $3 \times 10^9\ M_\odot$, roughly one-third of the interstellar hydrogen gas mass and about 2% of the dynamical mass of the galaxy at our assumed distance of 6 Mpc. The value of the CO(2–1)/CO(1–0) line ratio ranges from 0.35 to 2; 50% of the map is covered by very high ratio gas (>1). The very high ratios are predominantly from interarm regions and appear to indicate the presence of widespread optically thin gas. Star formation tracers are better correlated with the total neutral gas disk than with the molecular gas by itself, implying $\Sigma_{\rm SFR} \propto \Sigma_{\rm gas}$. Using the 100 μm and 21 cm continua from NGC 6946 as star formation tracers, we arrive at a gas consumption timescale of 2.8 Gyr, which is relatively uniform across the disk. The high star formation rate at the nucleus appears to be due to a large accumulation of molecular gas rather than a large increase in the star formation efficiency. The midplane gas pressure in the outer ($R > 10$ kpc) H I arms of NGC 6946 is close to the value at the radial limit (10 kpc) of our observed CO disk. If the midplane gas pressure is a factor for the formation of molecular clouds, these outer H I gas arms should contain molecular gas, which we do not see because this gas is beyond our detection limit.

Key words: galaxies: individual (NGC 6946) — galaxies: ISM — galaxies: spiral — ISM: molecules — stars: formation

1. INTRODUCTION

We have observed NGC 6946 as part of a program of deep mapping of extended, cold CO in nearby spiral galaxies (Crosthwaite et al. 2001, 2002). Large, fully sampled, and deep images of CO in nearby galaxies are relatively uncommon. Either interferometric images do not contain zero-spacing data (e.g., Sakamoto et al. 1999), or, if they do, the images typically do not go deep enough to detect cold, molecular disk gas. The detection of cold, extended molecular gas at large galactocentric radii in large spirals is a goal of this mapping project with the NRAO 12 m telescope.

A gas-rich Sc galaxy at a distance of 6 Mpc (Eastman et al. 1996; Sharina et al. 1997; Karachentsev et al. 2000), NGC 6946 is known for its bright and asymmetric optical spiral arms (Arp 1966). The pronounced asymmetry may be caused by interactions with neighboring dwarf galaxies, UGC 11583 and L149 (Sharina et al. 1997; Pisano & Wilcots 2000). NGC 6946 has a $9'$ optical diameter on the sky and an atomic hydrogen (H I) gas disk extending to $25'$ (Rogstad et al. 1973). Like many spirals, NGC 6946 has a central $\sim 2'$ diameter "hole" in its H I disk. Radio continuum, far-infrared (FIR), optical line, and X-ray observations indicate vigorous star formation in the disk and an interstellar medium (ISM) stirred by supernovae and stellar winds (Engargiola 1991; Boulanger & Viallefond 1992; Kamphuis & Sancisi 1993; Schlegel 1994; Lacey et al. 1997). The high level of star formation in the disk of NGC 6946 has been attributed both to its strong spiral density wave (Tacconi & Young 1990) and to stochastic, self-propagating star formation (DeGioia-Eastwood et al. 1984).

Until recently, the CO morphology beyond the inner $3'$ radius ($\sim$5 kpc) was not well known. Like many spiral galaxies, NGC 6946 has a bright nuclear CO peak which falls off nearly exponentially with galactocentric radius (Morris & Lo 1978; Young & Scoville 1982). A $3'$ diameter map of Tacconi & Young (1989) revealed substantial CO emission in the inner disk with several emission peaks. Casoli et al. (1990) mapped two $2'$ circular fields in the disk of NGC 6946 in a study of arm and interarm regions. The inner $2'$ region has been mapped with higher resolution single-dish and aperture-synthesis telescopes in transitions of CO and CO isotopomers (Ball et al. 1985; Weliachew et al. 1988; Sofue et al. 1988; Ishizuki et al. 1990; Wall et al. 1993; Regan & Vogel 1995). A larger interferometer+single-dish map of NGC 6946 has been made by the BIMA Survey of Nearby Galaxies team (Regan et al. 2001), although with lower sensitivity to cold extended emission than the maps we present here. Walsh et al. (2002) presented $21''$ resolution fully sampled single-dish maps of CO(1–0). We compare our results to theirs.

The on-the-fly (OTF) observing mode at the NRAO[1] was ideally suited to the imaging of extended gas in galaxies. Here we present $10' \times 10'$ maps of CO(1–0) and CO(2–1) covering the optical disk of NGC 6946 made with the 12 m telescope. The maps are deep enough to detect cold, extended interarm CO to levels of $I_{\rm CO} \sim 1$ K km s^{-1}, or $N_{\rm H_2} \sim 2 \times 10^{20}$ cm^{-2}. We use these primary tracers of the molecular gas phase and combine them with archival and published data in order to study the molecular gas disk, the total neutral gas surface density, and their relationship to star formation in the disk of NGC 6946.

[1] The National Radio Astronomy Observatory is a facility of the National Science Foundation operated under cooperative agreement by Associated Universities, Inc.

2. THE OBSERVATIONS AND DATA REDUCTION

2.1. 12 m CO *Observations*

The observations of CO(1–0) at 115 GHz and CO(2–1) at 230 GHz were made at the NRAO 12 m telescope at Kitt Peak on two separate observing runs in 1996 December and 1997 March. An equivalent of ~14 hr on-source observing was accumulated for each CO line. Calibration was by the chopper-wheel method (Ulich & Haas 1976). We convert the recorded T_r^* values (Kutner & Ulich 1981) to main-beam temperatures, $T_{\rm mb} = T_r^*/\eta_m^*$, with $\eta_m^* = 0.88 \pm 0.04$ at 115 GHz and $\eta_m^* = 0.56 \pm 0.06$ at 230 GHz (Mangum 1996b, 1997).[2] We report $T_{\rm CO} = T_{\rm mb}$ throughout this paper. The filter-bank spectrometer was configured for 2 MHz channel widths with 256 total channels, producing spectral channels of a 5.2 km s^{-1} width at 115 GHz and 2.6 km s^{-1} at 230 GHz.

The OTF observing mode was used (Mangum 1996a).[3] Scanning rates between 30″ s^{-1} and 40″ s^{-1} and scan row spacings of 18″ at 115 GHz and 8″ at 230 GHz were selected to ensure sampling better than Nyquist over the mapped 16′ × 10′ region. The beam size (FWHM) at 115 GHz is 55″, and 27″ at 230 GHz. Chopper-wheel calibration and sky off-source positions were measured every two scans. The rms noise level was reduced by averaging the 16 individual OTF maps made at 115 GHz and 10 individual OTF maps at 230 GHz.

The OTF data were gridded using the NRAO AIPS package. A linear baseline was removed from each spectrum. At this stage of the data reduction the background in the channel maps is uneven from one scan row to the next. This spatial variation, due to sky brightness fluctuations between successive off-source sky measurements, appears as "stripes" in the continuum level running in the scan direction. The maps were made large enough to give us emission-free, 2.5′ wide regions at the east and west ends of the maps, verified by the examination of individual spectra from these regions. These regions were used to remove a linear baseline from each row of the channel maps in the scan direction, effectively giving us a uniform background in all the channel maps. The rms variation in the channel maps before and after "destriping" differed by 10 mK at 115 GHz and 30 mK at 230 GHz; in both cases a 20% reduction in the channel map noise.

The mean rms noise (1 σ) from fully reduced, line-free channels is $T_{\rm mb} = 0.050$ K and $T_{\rm mb} = 0.145$ K for the CO(1–0) and CO(2–1), respectively. The channels were averaged to a 10.4 km s^{-1} channel width; the mean rms noise in the averaged channel maps is 0.035 K for CO(1–0) and 0.085 K for CO(2–1). The error beam of the 12 m telescope, which has been measured at 345 GHz, is extrapolated to be 8′–9′ FWHM (Mangum 1997). The contribution from the error beam in the individual channel maps is estimated to be less than a few percent, which we neglect here (see the discussion in Crosthwaite et al. 2002). In the 10.4 km s^{-1} channel width cubes the rescaled uncertainty in $T_{\rm mb}$ due to sky brightness fluctuations is ±7 mK for CO(1–0) and ±11 mK for CO(2–1).

We are interested in bringing out as much of the extended low-level CO emission as possible in our integrated intensity maps. To do this we want to minimize the noise that would normally be added to an $I_{\rm CO}$ map when the channel maps are added together. To test the effects of the level of flux cut (the level in the individual channels below which the data are deemed to be noise and are not added to the integrated map) on the final integrated flux, we did the following test. We convolved the CO cubes to twice the beam size and used the regions with emission >3 σ to create mask cubes. The mask cubes allow us to define areas of emission using smoothed, hence more sensitive images, which is one way of discriminating between signal and noise. We then created $I_{\rm CO}$ maps from both the masked and unmasked cubes using flux cuts from 1.0 σ to 0 σ in 0.1 σ decrements. The total flux in the CO(1–0) integrated intensity map made from the masked cube with a 0.5 σ flux cut agrees with flux from the unmasked cube with no flux cut, to within 1%. For the CO(2–1) map, a more conservative 0.8 σ was used.

We created maps of the per-pixel uncertainty for our $I_{\rm CO}$ maps by combining the per-channel sky brightness fluctuation and rms noise, counting the number of channels contributing to the integrated emission at each pixel, and then adding the uncertainty in η_m^* using error analysis techniques for the sums and products of independent variables. We created maps of the fractional uncertainty in our integrated intensity maps by dividing the aforementioned uncertainty maps by the $I_{\rm CO}$ maps themselves. The uncertainty is dominated at the nucleus by the uncertainty in η_m^*, while at the outer edges of the maps the uncertainty is dominated by the rms noise. For the CO(1–0) integrated intensity map the combined uncertainty is on the order of 7% at the nucleus, 12% along the prominent spiral arm pattern, and 25% for the outer disk emission. For the CO(2–1) map the uncertainties are on the order of 11% at the nucleus, 20% along the spiral arm pattern, and 30% for the outer disk emission.

To obtain H_2 column densities from $I_{\rm CO}$ we applied the "standard conversion factor," $X_{\rm CO}$ (Scoville & Sanders 1987; Young & Scoville 1991); $X_{\rm CO}$ is estimated to be accurate to a factor of 2 in the Milky Way disk (Solomon et al. 1987 and references therein), although it may overpredict $N_{\rm H_2}$ in the central arcminute of large spirals (Dahmen et al. 1998; Meier & Turner 2001). We assume that these uncertainties hold for NGC 6946 as well. We will adopt the standard conversion factor,

$$X_{\rm CO} = N_{\rm H_2}/I_{\rm CO} = 2 \times 10^{20}\ {\rm cm^{-2}}\ \left({\rm K\ km\ s^{-1}}\right)^{-1},$$

of Strong et al. (1988) throughout the remainder of the paper [a recent calibration by Hunter et al. (1997) finds a mean $X_{\rm CO} = 1.6 \times 10^{20}$ cm^{-2} (K km s^{-1})$^{-1}$ for the entire Milky Way disk and $X_{\rm CO} = 2.7 \times 10^{20}$ cm^{-2} (K km s^{-1})$^{-1}$ for the outer disk, $R > 1\ R_\odot$]. Using this conversion factor, $I_{\rm CO}$ can be converted into H_2 (no He or heavier elements) surface densities using

$$\Sigma_{\rm H_2}\left(M_\odot\ {\rm pc^{-2}}\right) = 2.4\left(I_{\rm CO}/1\ {\rm K\ km\ s^{-1}}\right),$$

including a geometric correction for the inclination of the galaxy (40°; Table 1)[4] to correct the surface densities to their face-on values.

2.2. H I, 21 cm *Continuum, and FIR Maps*

We obtained archival VLA D-configuration 21 cm observations of the H I line in NGC 6946, which are described in Tacconi & Young (1986). The beam size is 49″ × 42″, with P.A. = 73°, and each channel has a velocity width of 10.3 km s^{-1}. The integrated intensity map was constructed from signals greater than 1.7 mJy beam^{-1} (1.2 σ). Absolute flux calibration error is on the order of the uncertainty in the flux of 3C 286, <5%. The single-channel rms noise of 1.4 mJy beam^{-1} corresponds to an H I column density of 7.7×10^{18} cm^{-2}.

[2] Available at http://www.tuc.nrao.edu/12meter/obsinfo.html.
[3] Available at http://www.tuc.nrao.edu/12meter/obsinfo.html.
[4] The adopted inclination was derived from a Brandt model fit to the H I data.

TABLE 1
GLOBAL PROPERTIES OF NGC 6946

Property	Value
Hubble type[a]	Scd
R.A. (J2000.0)[b]	$20^h34^m51.6^s \pm 0.4^s$
Decl. (J2000.0)[b]	$60°9'8.7'' \pm 1.6''$
l[a]	95.7°
b[a]	11.7°
Distance[c]	6 Mpc
v_{LSR}[d]	50.5 ± 1.3 km s^{-1}
Inclination[d]	$40° \pm 10°$
Position angle[d]	$242° \pm 1°$
V_{max}[d]	170 ± 40 km s^{-1}
$R_{V_{max}}$[d]	$5.1' \pm 0.7'$ (9.0 kpc)
n[d]	1.07 ± 0.07
$M_{H_2,total}$[e]	$3.3 \times 10^9\ M_\odot$
$M_{H\,I,observed}$[f]	$5 \times 10^9\ M_\odot$
$M_{H\,I}$[g]	$7 \times 10^9\ M_\odot$
M_{gas}[h]	$1.4 \times 10^{10}\ M_\odot$
M_{dyn}[i]	$1.9 \times 10^{11}\ M_\odot$

[a] Obtained from the NASA/IPAC Extragalactic Database.
[b] Dynamical center based on fit of the Brandt rotation model to the H I data.
[c] Sharina et al. (1997).
[d] Kinematic parameters from fit of the Brandt rotation model to the H I data.
[e] Detected using a 2.0×10^{20} K km s^{-1} conversion factor.
[f] Detected; no VLA missing flux estimate.
[g] Includes VLA missing flux estimate.
[h] Includes factor for He and heavier elements: $1.36(M_{H_2} + M_{H\,I})$.
[i] Total dynamical mass based on Brandt model fit parameters.

Integrated intensities were converted to face-on H I surface densities (no He or heavier elements) using

$$\Sigma_{H\,I} = 3.3\ M_\odot\ \mathrm{pc}^{-2}\ \left(\mathrm{Jy\ beam}^{-1}\ \mathrm{km\ s}^{-1}\right)^{-1} I_{H\,I}.$$

From a comparison to the single-dish observations of Gordon et al. (1968), we estimate that 40% of the H I flux of NGC 6946 is missing from the VLA maps due to the lack of short baselines (emission extended over 15′). If the missing flux exists as a screen across the disk of NGC 6946, it constitutes a missing uniform H I surface density of $\sim 1.2\ M_\odot$ pc^{-2}.

The total observed H I emission in the VLA maps amounts to $M_{H\,I} = 5 \times 10^9\ M_\odot$, not including missing undersampled emission. Tacconi & Young (1986), using the same VLA H I data, obtained $3.9 \times 10^9\ M_\odot$, rescaled to $D = 6$ Mpc. Their mass is probably slightly lower than ours because they used a higher flux cutoff to produce their integrated intensity map. Boulanger & Viallefond (1992) obtained $6.7 \times 10^9\ M_\odot$ (rescaled to 6 Mpc). Boulanger's mass includes single-dish observations merged with the Westerbork interferometer data to cover the short spacings and corrections for Milky Way absorption and emission. The difference between our mass and theirs, 33%, is in line with our estimate of the missing flux in the VLA map.

A Brandt rotation curve was fit to the H I radial velocities, for radii $<10'$. Our resulting kinematic parameters, shown in Table 1, are in good agreement with the rotation parameters found by Carignan et al. (1990). A total dynamical mass estimate based on the fit (see Table 1) is $M_{dyn} = (1.9 \pm 0.6) \times 10^{11}\ M_\odot$.

We produced a 21 cm continuum map by averaging four line-free channels in the NGC 6946 H I channel cube. The 1 σ noise level is 1.2 mJy beam^{-1}.

High-resolution (HiRes) 60 and 100 μm *IRAS* maps were obtained from IPAC.[5] The 100 μm HiRes map was produced by 200 iterations of a maximum entropy method, yielding a $69'' \times 65''$, P.A. $= 20°$ beam and a 1 σ noise level of 2.0 MJy sr^{-1}. The 60 μm HiRes map was produced by 50 iterations of a maximum entropy method, yielding a $45'' \times 41''$, P.A. $= 21°$ beam and a 1 σ noise level of 0.6 MJy sr^{-1}.

3. IMAGES OF CO IN NGC 6946: THE MOLECULAR GAS

A relatively heavy molecule, CO is easily excited at the temperatures of molecular clouds, with its first rotational level at an energy of $E/k = 5.5$ K. Since it has a small dipole moment and is generally optically thick, the excitation of the CO rotational levels is driven by collisions at H_2 densities above $n_{crit} \sim 300$ cm^{-3} for the $J = 1$–0 transition. The $J = 2$–1 transition, with an upper level energy of $E/k = 16.6$ K, has a higher critical density, although its higher optical depth somewhat compensates for that. For gas kinetic temperatures of $\sim$7–10 K, we expect CO(2–1) to be thermalized at critical densities above $n_{crit} \sim 10^3$ cm^{-3}, slightly higher than CO(1–0) values. One might therefore expect CO(2–1) emission to be more tightly confined to the spiral arms than CO(1–0), since the arms probably have denser gas and are also closer to H II regions that might warm the clouds (e.g., Scoville et al. 1987). However, as we shall see, the CO(2–1) and CO(1–0) properties in NGC 6946 are not precisely what one might expect based on Galactic clouds.

We do not present CO kinematic data (radial velocity maps, velocity dispersion maps, and rotation curves). Our kinematic results do not differ significantly from those of Walsh et al. (2002), and we refer the reader to their presentation of the kinematics of NGC 6946 derived from IRAM single-dish data.

3.1. CO(1–0) *Maps*

The 24 CO(1–0) channels containing line emission are displayed in Figure 1. The channels have been smoothed to a 10.4 km s^{-1} channel width. The channel maps show the butterfly pattern characteristic of emission from an inclined rotating disk. High-velocity nuclear gas shows up as emission at the location of the nucleus spread across nearly the entire bandwidth of the line emission.

The disk of CO emission in NGC 6946 extends 8′ (14 kpc) north-south by 10′ (18 kpc) east-west, as shown in the integrated intensity ($I_{10} = \int T_{10}\, dv$; Fig. 2*a*) and the peak main-beam brightness temperature maps (T_{10}; Fig. 2*b*). Walsh et al. (2002) also found CO emission extended out to 10′ in 22″ resolution single-dish IRAM observations. There are no significant differences between our and Walsh's map that cannot be attributed to the difference in resolution. The CO(1–0) emission covers the entire optical disk of a Digitized Sky Survey (DSS) image of NGC 6946 (Fig. 2*c*).

The total CO(1–0) flux density measured over a velocity width of 250 km s^{-1} is $(1.2 \pm 0.3) \times 10^4$ Jy km s^{-1}, in agreement with the value published in the FCRAO survey of $(1.2 \pm 0.4) \times 10^4$ Jy km s^{-1} (Young et al. 1995) but higher than the $(0.79 \pm 0.01) \times 10^4$ Jy km s^{-1} detected in a 22″ resolution single-dish IRAM map (Walsh et al. 2002). Converting our total observed I_{10} into a total molecular mass, we obtain $M_{H_2} = 3.3 \times 10^9\ M_\odot$ for NGC 6946; the mass will be higher if there is outer disk CO that we do not detect. This is consistent with the mass obtained by Tacconi & Young (1989), $3.0 \times 10^9\ M_\odot$ (rescaled to 6 Mpc and our X_{CO}).

[5] Descriptions of the *IRAS* HiRes data reduction and HiRes data products are available at http://irsa.ipac.caltech.edu/IRASdocs/hires_over.html.

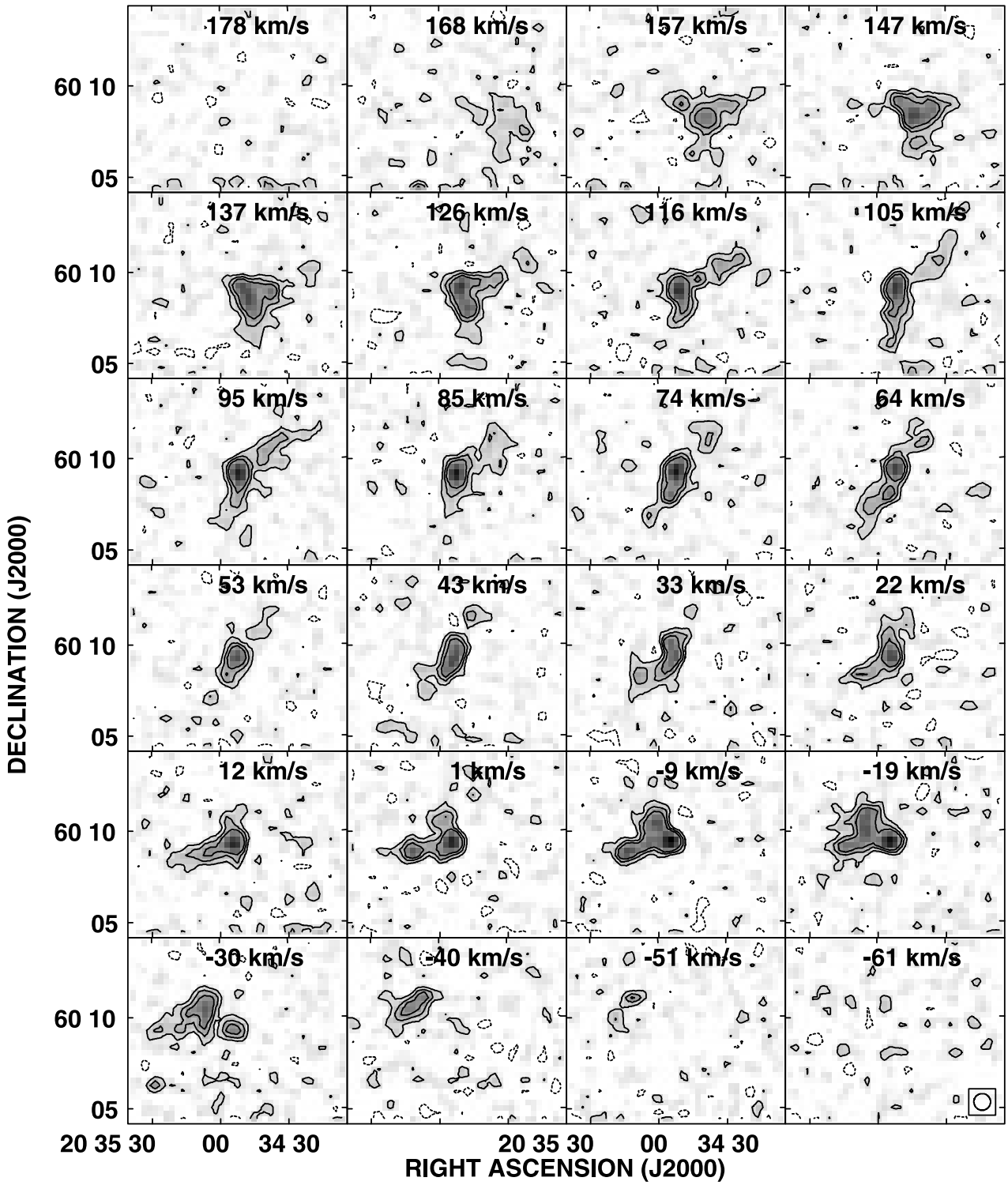

FIG. 1.—CO(1–0) channel maps for NGC 6946. The gray scale ranges from 0 to 0.54 K. Contours are at −0.070, 0.070, 0.14, and 0.21 K. The rms noise in a channel with no emission is 0.033 K. The 55″ (FWHM) circular beam is displayed in the −61 km s^{-1} channel at the lower right. Each channel is labeled with the channel velocity (LSR). The channels are separated by 10.4 km s^{-1}.

The CO integrated intensity (I_{10}) and temperature maps (T_{10}) both show the same features: a bright nucleus, a broad asymmetrical spiral arm pattern, and an overall asymmetrical distribution of the disk emission. The nucleus has a CO emission peak at $\alpha = 20^{\rm h}34^{\rm m}52.6^{\rm s}$, $\delta = 60°9'16''$ (J2000.0), with $I_{10}^{\rm nuc} = 72$ K km s^{-1}, $N_{\rm H_2}^{\rm nuc} = 1.4 \times 10^{22}$ cm^{-2}, or in terms of surface density, $\Sigma_{\rm H_2}^{\rm nuc} = 170\ M_\odot$ pc^{-2} (face-on value), averaged over our 1.6 kpc diameter beam. The total molecular mass within the central beam is $4.7 \times 10^8\ M_\odot$. Ishizuki et al. (1990) obtained $4.5 \times 10^8\ M_\odot$ (adjusted to 6 Mpc and our conversion factor) in a 65″ diameter region from interferometric observations that recovered 70% of the total flux. Large-scale CO spiral structure is traced in a broad S-pattern, outlined by the 7.5 K km s^{-1} contour in the I_{10} map and more clearly seen in the T_{10} map, outlined by the 0.23 K contours. Here, molecular gas surface density is $>20\ M_\odot$ pc^{-2}. There is also extended, weaker CO emission from the disk outside of

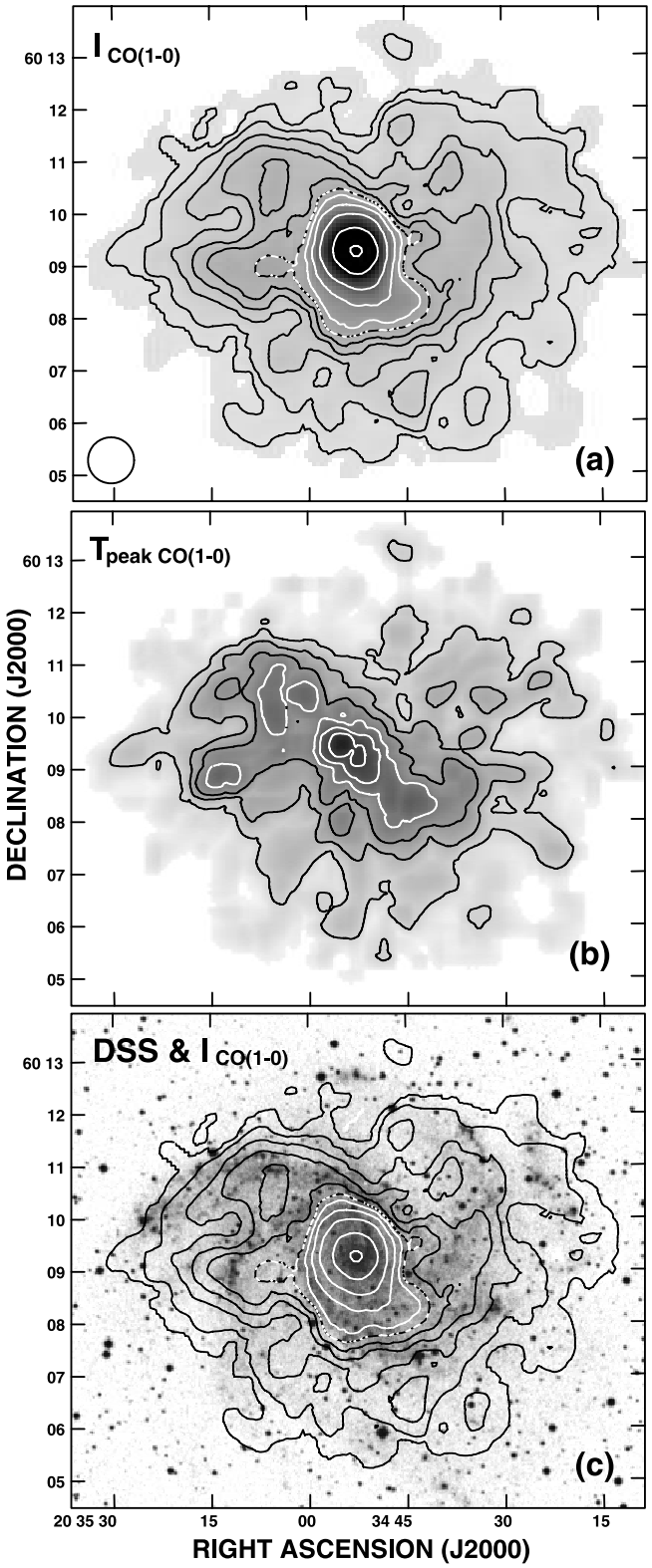

FIG. 2.—CO(1–0) integrated and peak intensity maps for NGC 6946. (*a*) CO(1–0) integrated intensity map. The gray scale ranges from 0 to 50 K km s^{-1}. The contour levels are 1, 2.5, 5, 7.5, 10, 12.5, 15, 20, 30, 50, and 70 K km s^{-1}. The 55″ (FWHM) circular beam is displayed at the lower left. (*b*) CO(1–0) peak intensity map. The gray scale ranges from 0 to 0.52 K. The contour levels are 0.10, 0.17, 0.23, 0.30, 0.37, and 0.43 K. (*c*) DSS uncalibrated optical image with the same I_{10} contours shown in (*a*).

the 7.5 K km s^{-1} contour in the I_{10} map. Large regions of molecular gas exist to the northwest and southeast of the nucleus, as well as patchy emission out to the edges of the maps. Not all of this gas is associated with the weaker optical arm pattern. The face-on gas surface density for this extended region has a mean I_{CO} of $I_{10} \sim 3$ K km s^{-1}, corresponding to $N_{H_2} = 5 \times 10^{20}$ cm^{-2} or $\Sigma_{H_2} \sim 10\ M_\odot$ pc^{-2}. This extended portion of the gas disk contributes one-fourth of the total CO emission we observe. The total mass of this extended gas disk is $M_{H_2} \sim 10^9\ M_\odot$.

3.2. CO(2–1) *Maps*

The 24 channels containing CO(2–1) emission are displayed in Figure 3. The rms of these 10.4 km s^{-1} channels is 3 times as high as for CO(1–0), so the maps are less sensitive to faint emission. The total CO(2–1) flux density measured over a velocity width of 250 km s^{-1} is $(3.5 \pm 1.0) \times 10^4$ Jy km s^{-1}. The butterfly patterns for the CO(2–1) and CO(1–0) are generally the same, with the differing resolutions, 27″ and 55″, respectively, accounting for most of the differences.

As with CO(1–0) the bright nucleus and asymmetric distribution of arm and disk emission are also apparent in the integrated intensity (I_{21}) and peak main-beam brightness temperature maps (T_{21}) (Figs. 4*a* and 4*b*). The CO(2–1) emission in NGC 6946 is almost as extensive as that of the CO(1–0): the north-south and east-west dimensions are only 1′ shorter. The observed CO(2–1) emission covers the brighter portions of the DSS optical image of NGC 6946 (Fig. 4*c*).

The nuclear peak of the CO(2–1) integrated intensity map is at $\alpha = 20^h34^m53.1^s$, $\delta = 60°9'15''$ (J2000.0), with $I_{21}^{nuc} = 125$ K km s^{-1}. Using a Galactic disk X_{CO}, this corresponds to a peak column density of $N_{H_2}^{nuc} = 2.2 \times 10^{22}$ cm^{-2}, or 450 $M_\odot$ pc^{-2} averaged over the 790 pc beam. If other nearby galaxies are any indication, this may be an overestimate of the true molecular gas mass in the nucleus by a factor of ~2–3 (§ 3.1.) The largest T_{21} value, 0.85 K, occurs at the same location as the I_{21} peak, and both peaks are consistent with the location of the I_{10} peak.

At the presented resolution of the maps, inside a 2′ (3.5 kpc) radius both the CO(2–1) and CO(1–0) emission trace a broad two-arm pattern. At a 2.5′ radius (4.4 kpc) the CO(2–1) still traces a broad two-arm pattern, while the CO(1–0) emission from a larger beam has clearly bifurcated into a four-arm spiral (Fig. 5*a*). At a 3.5′ radius (6.1 kpc) five arms are discernible in azimuthal emission plots of both CO emission lines (Fig. 5*b*).

Along the optical arm pattern the CO(2–1) emission is uneven (Fig. 4*c*), with typical variations of 15 and 5 K km s^{-1} separated by 40″ or less. This same clumpy pattern of CO arm emission can be seen in the 22″ CO(1–0) and CO(3–2) maps presented by Walsh et al. (2002). The emission on each arm at the same galactocentric radius is also uneven, as can be seen in Figure 5.

At 27″ resolution it becomes possible to distinguish between arm and interarm emission. The I_{21} contrast between the brighter on-arm clumps and obvious off-arm regions is ~3. Using the DSS optical image to mask the outer ($R > 2.5'$) arm/interarm regions, we obtain a mean arm/interarm contrast of 2.4. This is higher than both the 1.2 and 1.8 values found from the CO(1–0) and CO(3–2) IRAM observations of Walsh et al. (2002), who interpret the increase in contrast at the higher CO transitions versus CO(1–0) as evidence that the on-arm molecular gas is warmer.

The presence of widespread interarm gas becomes plainly apparent in a comparison to an optical image, Figure 4*c*. The fact that interarm CO(2–1) is present and at emission levels comparable to CO(1–0) suggests that the interarm gas is also not very cold and that it must be warmer than ~4–7 K. This widespread

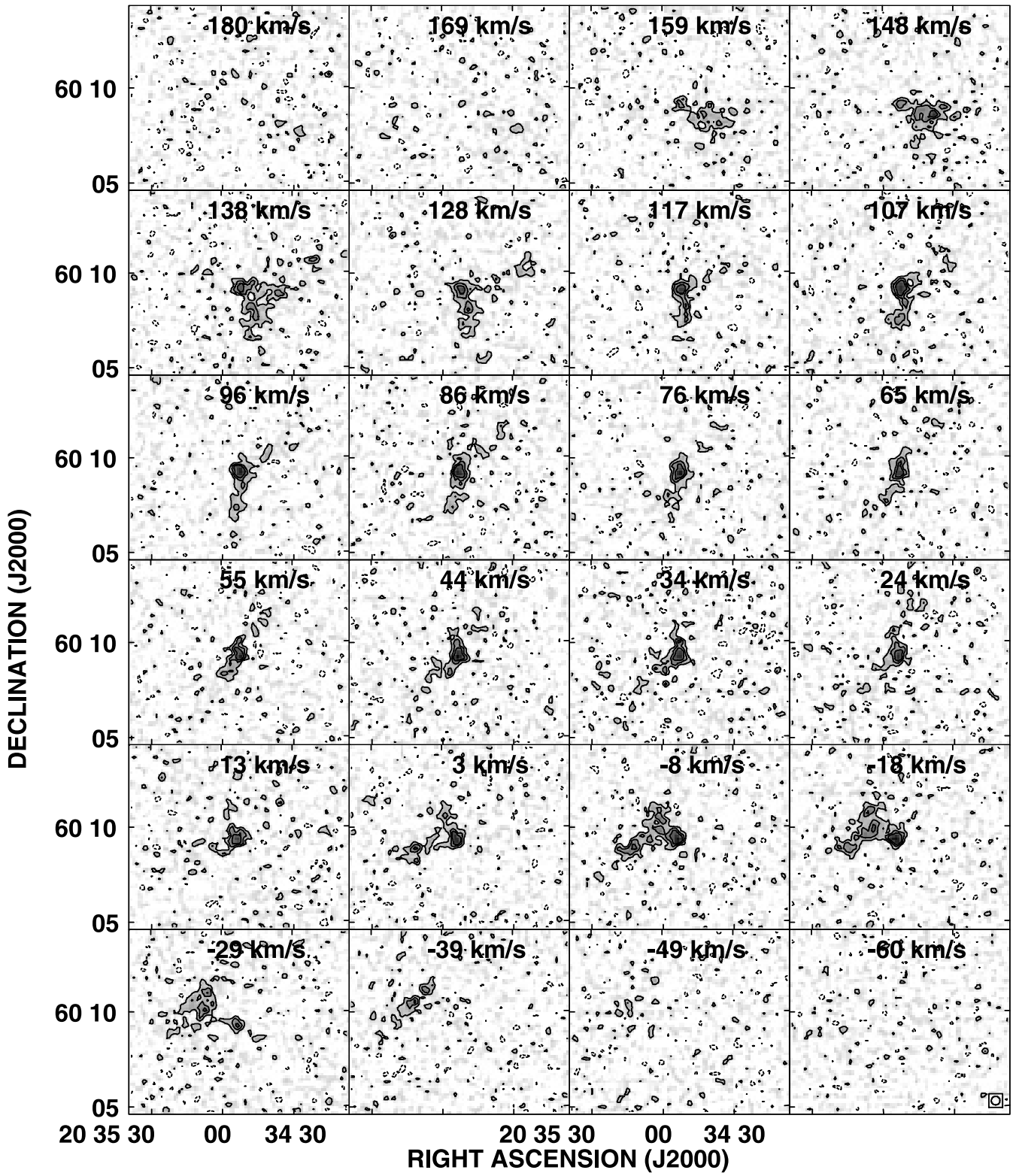

FIG. 3.—CO(2–1) channel maps for NGC 6946. The gray scale ranges from 0 to 0.85 K. Contours are at −0.17, 0.17, 0.34, and 0.51 K. The rms noise in a channel with no emission is 0.085 K. The 27″ (FWHM) circular beam is displayed in the −60 km s^{-1} channel at the lower right. Each channel is labeled with the channel velocity (LSR). The channels are separated by 10.4 km s^{-1}.

distribution of interarm gas is not seen in the Sakamoto et al. (1997) CO(2–1) survey of the Milky Way.

3.3. *Excitation of* CO *in NGC 6946*

A CO ratio map, $r_{12} = I_{21}/I_{10}$, is presented in Figure 6*a*. The CO(2–1) channel cube was convolved to the beam size of the CO(1–0) data, and the >3 σ emission from the beam-matched cubes was used to produce the r_{12} map. The spiral pattern is only weakly reflected in the r_{12} map. Outside of the inner few arcminute radius the pattern breaks up into a patchwork of high- and low-r_{12} regions.

The ratio uncertainty for the regions of strong emission is dominated by the error in the conversion to main-beam temperature,

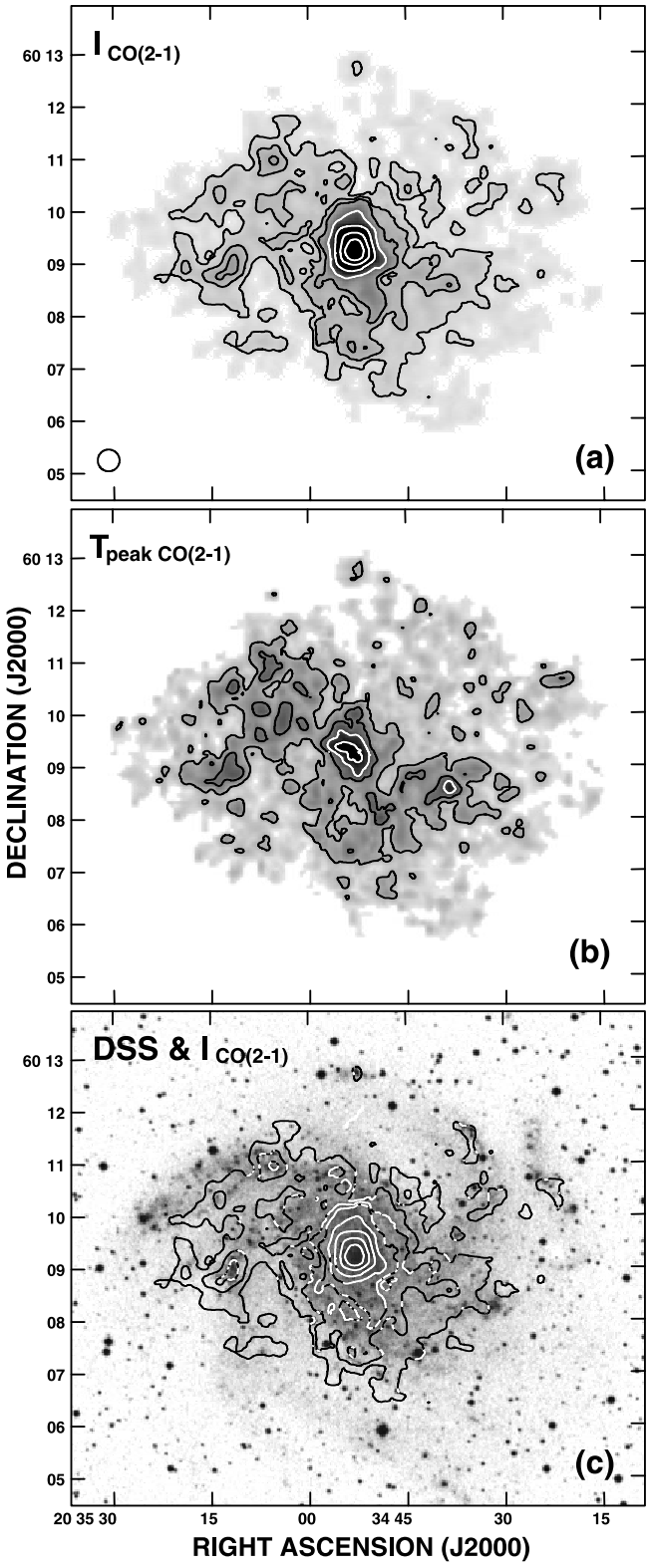

FIG. 4.—CO(2–1) integrated and peak intensity maps for NGC 6946. (*a*) CO(2–1) integrated intensity map. The gray scale ranges from 0 to 50 K km s^{-1}. The contour levels are 5, 10, 15, 30, 50, 75, and 100 K km s^{-1}. The 27″ (FWHM) circular beam is displayed at the lower left. (*b*) CO(2–1) peak intensity map. The gray scale ranges from 0 to 0.8 K. The contour levels are 0.26, 0.43, 0.60, and 0.77 K. (*c*) DSS uncalibrated optical image with the same I_{21} contours shown in (*a*).

while the uncertainty for the weaker emission regions is dominated by the rms noise in the contributing channels of emission. Adding in quadrature the fractional uncertainties from the I_{CO} maps, we obtain an error estimate on the order of 15% at the nucleus, 25% along the spiral arm pattern, and 40% for the outer disk ratios. We were concerned that the ratio might be biased toward higher values due to the uncertainty in the denominator. We performed a standard statistical analysis to correct the ratio for this bias. The bias-corrected r_{12} map was not significantly different from the map presented in Figure 6*a* and well within our reported error. Despite the large uncertainty estimates, our ratios are consistent with those derived from other independent observations (Weliachew et al. 1988; Ishizuki et al. 1990; Casoli et al. 1990; Wall et al. 1993).

In principle, r_{12}, the ratio of CO(2–1) to CO(1–0) integrated intensities, gives information on the excitation of the CO emission and, depending on circumstances, the kinetic temperature T_k. The observed main-beam temperature at frequency ν is related to a Planck function B_ν, with excitation temperature T_{ex}, by the areal beam filling factor f_a, a conversion to the Rayleigh-Jeans temperature scale, and radiative transfer through an optical depth τ_ν,

$$T_{mb} = f_a \frac{c^2}{2k\nu^2}[B_\nu(T_{ex}) - B_\nu(T_{cmb})](1 - e^{-\tau_\nu}),$$

including a correction for the cosmic microwave background contribution to the beam, $B_\nu(T_{cmb})$, at temperature 2.73 K. Standard assumptions are that f_a is the same for both emission lines, that both lines are optically thick ($\tau_\nu \gg 1$), and that the emission can be characterized by a single T_{ex} (Dickman et al. 1986; Maloney & Black 1988; Sakamoto 1996). With these assumptions we can naively derive T_{ex} values for the emission: $r_{12} = 0.9$ corresponds to $T_{ex} = 20$ K, while $r_{12} = 0.5$ corresponds to $T_{ex} = 3.5$ K. Higher ratio values are found in the nuclear regions of starburst galaxies where elevated star formation heats the molecular gas; lower values are typical of cold or subthermally excited ($T_{ex} < T_k$) disk molecular clouds. Values of $r_{12} > 1$ indicate optically thin gas in this picture.

Within 1′ of the nucleus, $r_{12} \sim 0.8$. This is consistent with other studies (Weliachew et al. 1988; Ishizuki et al. 1990; Wall et al. 1993) that indicate the presence of relatively dense molecular gas at temperatures of about $T_{ex} \sim 10$–15 K. This is comparable to the Milky Way mean r_{12} of 0.74 (Oka et al. 1996, 1998).

Along the optical arms the mean r_{12} is 0.83, ranging from 0.44 to 1.4. To within our uncertainties, this is the same as the 0.73 mean found for Milky Way molecular arms, where a similar range of r_{12} values is found (Sakamoto et al. 1995, 1997). From a naive interpretation of the ratios, a mean T_{ex} of 12 K is implied for the arm CO in NGC 6946.

Casoli et al. (1990) concluded that the interarm r_{12} does not differ significantly from that of the arms based on observations of two circular regions in the arms, one on the east side of NGC 6946, the other on the west side. The two circular regions they observed have a mean r_{12} of 0.8 in our ratio map, also not significantly different from that of the arm regions. However, when larger regions of the CO disk are sampled, a very different picture emerges. There are regions (5% of the ratio map) where $r_{12} < 0.6$, indicating cold ($T_{ex} < 5$ K) or subthermally excited CO. There are also much larger regions, where $r_{12} > 1$.

Very high ratio ($r_{12} > 1$) gas covers 50% of our ratio map; these are predominantly interarm regions (Fig. 6*b*). We have eliminated the possibility that these very high ratios are due to contributions from the telescope error beam at 230 GHz: the error beam

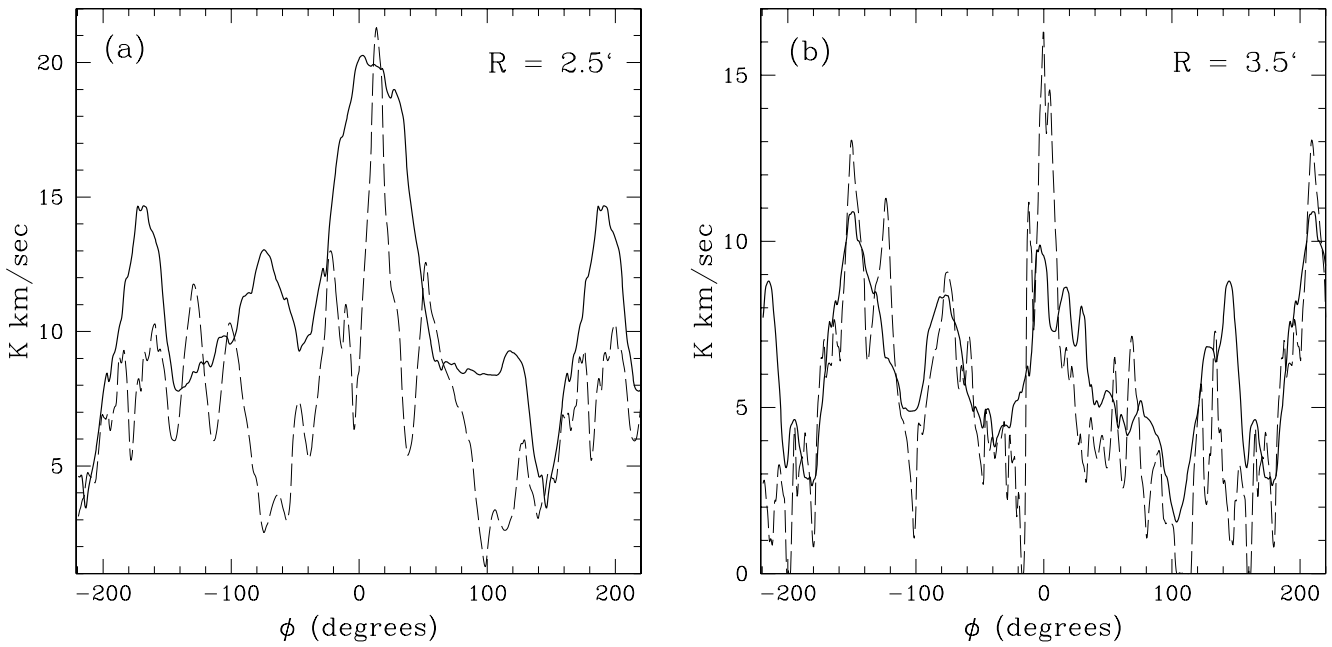

FIG. 5.—Azimuthal plots of CO in NGC 6946 at selected radii. The I_{CO} maps were transformed to face-on images, and the azimuthal variation in I_{CO} was measured at constant galactic radii. Due south is at $\phi = 0^{\circ}$, and west is at $\phi = 90^{\circ}$. CO(2–1) is traced by the dashed line, and CO(1–0) by the solid line. The data are presented at their native beam sizes, 27″ and 55″, for the CO(2–1) and CO(1–0) emission, respectively. (*a*) Azimuthal variation at $R = 2.5'$ (4.4 kpc). (*b*) Azimuthal variation at $R = 3.5'$ (6.1 kpc).

at the 12 m telescope is a measured quantity, and modeling of the error beam contribution in the individual channel maps shows that it contributes at most a few percent of the emission in the I_{21} map.

The high r_{12} ratios appear to indicate the presence of widespread, warm, optically thin CO-emitting gas in the interarm regions. While optically thin CO emission is not typical of Galactic molecular clouds, our large beam and unusual perspective from outside the disk of NGC 6946 may allow us to trace a component that is difficult to detect in the Galaxy. We note that the photon-dominated regions around cool stars can produce bright CO emission with high temperatures (Spaans et al. 1994), since their softer radiation fields allow the CO to be photoelectrically warmed at low A_v. Also, as pointed out by Wiklind et al. (1990) it does not take much optically thin gas to swing the emissivity; the CO(2–1) emission that we see could easily come from a small amount of optically thin but CO-loud gas that is not the dominant cloud population. Other less likely possibilities are discussed in Crosthwaite et al. (2002).

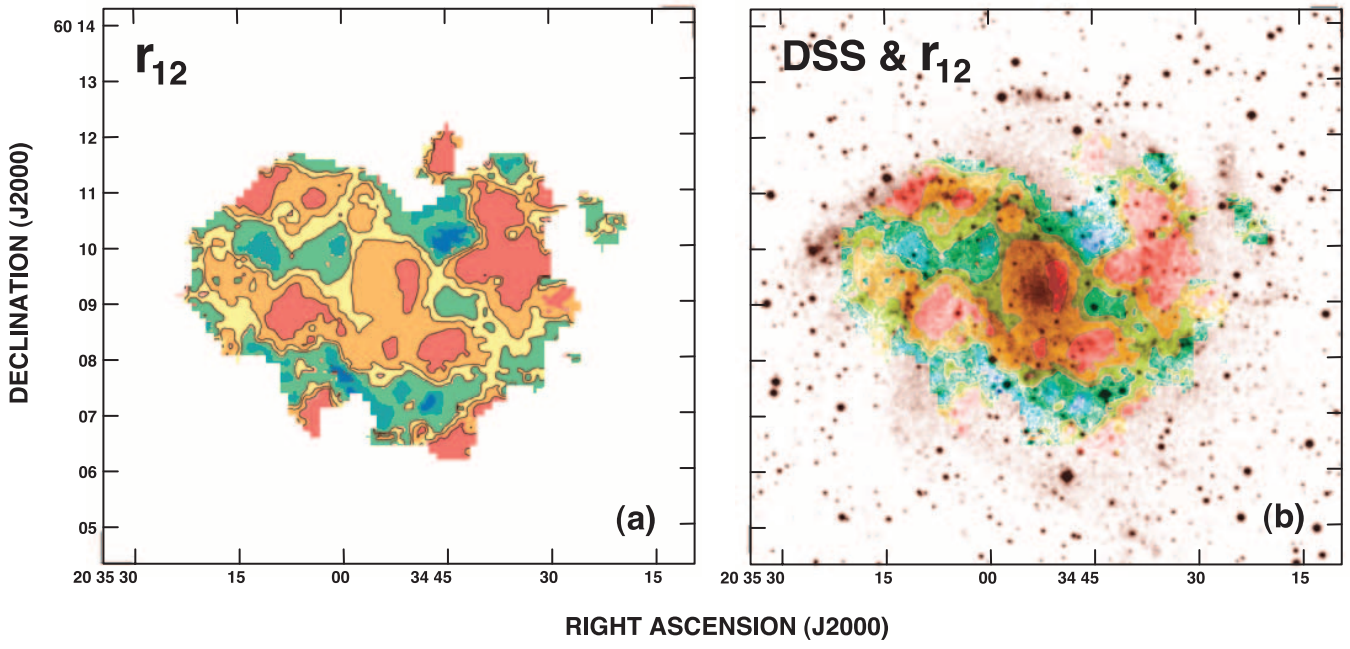

FIG. 6.—CO(2–1)/CO(1–0) ratio in NGC 6946. (*a*) Plot of $r_{12} = I_{21}/I_{10}$. The contours are at $r_{12} = 0.8$, 1.0, and 1.2. For the colored regions, red is for $r_{12} < 0.8$, orange for $0.8 > r_{12} > 1.0$, yellow for $1.0 > r_{12} > 1.2$, green for $r_{12} > 1.2$, and blue for $r_{12} \sim 2$. (*b*) DSS optical image with r_{12} in color. The color scheme roughly follows that of (*a*) and is intended to show the relationship between the regions of high/low r_{12} and the optical stellar disk.

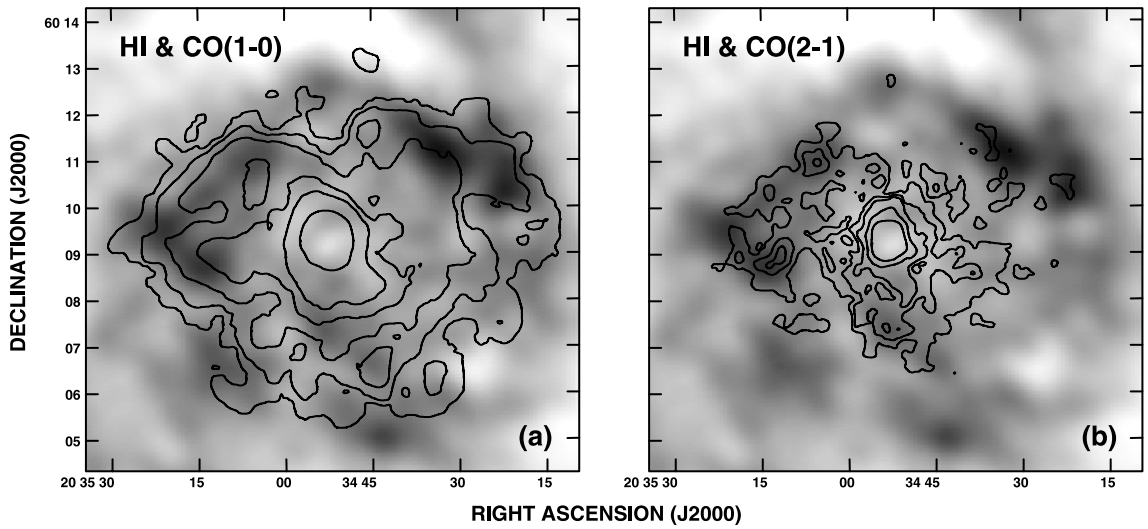

FIG. 7.—CO and H I in NGC 6946. (*a*) $I_{\rm H\,I}$ (*gray scale*) and I_{10} (*contours*). The gray scale ranges from 0.5 to 3.7 Jy beam^{-1} km s^{-1}. The I_{10} contours are at 1, 2.5, 5, 10, 15, and 35 K km s^{-1}. (*b*) $I_{\rm H\,I}$ (*gray scale*) and I_{21} (*contours*). The gray scale ranges from 0 to 3.7 Jy beam^{-1} km s^{-1}. The I_{21} contours are at 5, 10, 15, 30, and 50 K km s^{-1}.

We have also seen a high overall $r_{12} \sim 1$ in M83 (Crosthwaite et al. 2002), confirming earlier reports of unusually high r_{12} in M83 and NGC 6946 (Castets et al. 1990; Wiklind et al. 1990). Large-scale r_{12} maps of the Milky Way (Sakamoto et al. 1995, 1997; Oka et al. 1996, 1998) show high ratios in immediate proximity to pockets of star formation. The widespread regions of high r_{12} seen in M83 and NGC 6946 are not seen in surveys of CO in our Galaxy.

4. CO, H I, AND THE NEUTRAL GAS SURFACE DENSITY

Although CO emission covers only 15% of the H I disk surface area, NGC 6946 is nevertheless a molecular-gas-rich galaxy; one-third of the hydrogen gas disk is in molecular form. This is consistent with the 36% value from Walsh et al. (2002) once the flux missed in the interferometer H I maps is taken into account.

In Figure 7*a* we present our CO(1–0) emission in contours superimposed on a gray-scale image of the H I emission. This image shows that CO emission fills the inner 6′ of the H I disk. The H I disk has a central depression, which rises to peaks in a clumpy ring of emission. The H I ring is coincident with the outer boundary of CO(1–0). While spiral structure is readily apparent in the outer H I disk (Tacconi & Young 1986), it is insignificant in the inner disk, $R < 5'$ (9 kpc), where the H I column densities decline and H_2 takes over. At 1′ resolution there are no obvious systematic displacements of the H I relative to the CO(1–0) spiral structure other than that the strongest H I tends to be near the outermost ends of the CO(1–0) arms. In fact, if anything, the H I and CO peaks tend to coincide, which is more apparent in the higher resolution CO(2–1) maps.

The CO(2–1) image in contours is shown in Figure 7*b*, again with a gray-scale image of H I. Outside the inner 2′ (3.5 kpc) region of the H I depression, the peaks of CO(2–1) emission tend to coincide with H I peaks along the ring. This could be evidence for photodissociated H_2 creating a higher H I column density at these locations. Tilanus & Allen (1989, 1993) and Wilson & Scoville (1991) suggest the same explanation for H I in the spiral arms of M51, M83, and M33.

From these images we have constructed plots of the azimuthally averaged gas surface densities, Σ_{H_2}, $\Sigma_{\rm H\,I}$ and $\Sigma_{\rm gas}$, as a function of galactocentric radius in Figure 8 (corrected for inclination). This is similar to the plot of Young & Scoville (1982), which was based on a radial cross map, and those of Tacconi & Young (1986) and Walsh et al. (2002). H_2 dominates the neutral gas distribution within the central 3′ (5 kpc) of NGC 6946, rapidly fading into a predominantly H I disk beyond. A least-squares fit of an exponential to $I_{\rm CO}$ over the entire range of radii has a scale length of $1.0' \pm 0.1'$ (1.8 kpc). Tacconi & Young (1986) and Walsh et al. (2002) obtained scale lengths of 1.5′ and 1.4′ for the CO disk from FCRAO and IRAM single-dish observations; Regan et al. (2001) obtained 1.3′ from the BIMA interferometer survey data combined with NRAO 12 m telescope observations. All these latter scale lengths exclude the nuclear contribution to the fit and are sensitive to the range of radii over which they were computed. We obtain 1.2′ and 1.3′ fitting to the

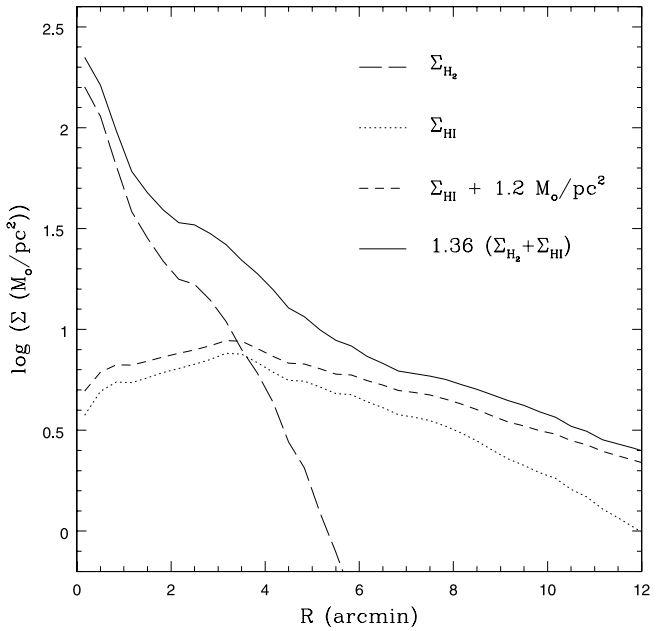

FIG. 8.—Gas surface density vs. radius in NGC 6946. Plotted are Σ_{H_2} derived using the standard conversion factor; $\Sigma_{\rm H\,I}$ from the observed emission; $\Sigma_{\rm H\,I}$ increased for the VLA missing flux estimate; and the total gas surface density increased by a factor of 1.36 to include the He and heavier element content. All have been corrected for inclination ($\cos i$). At our assumed distance of 6 Mpc, $1' = 1.75$ kpc.

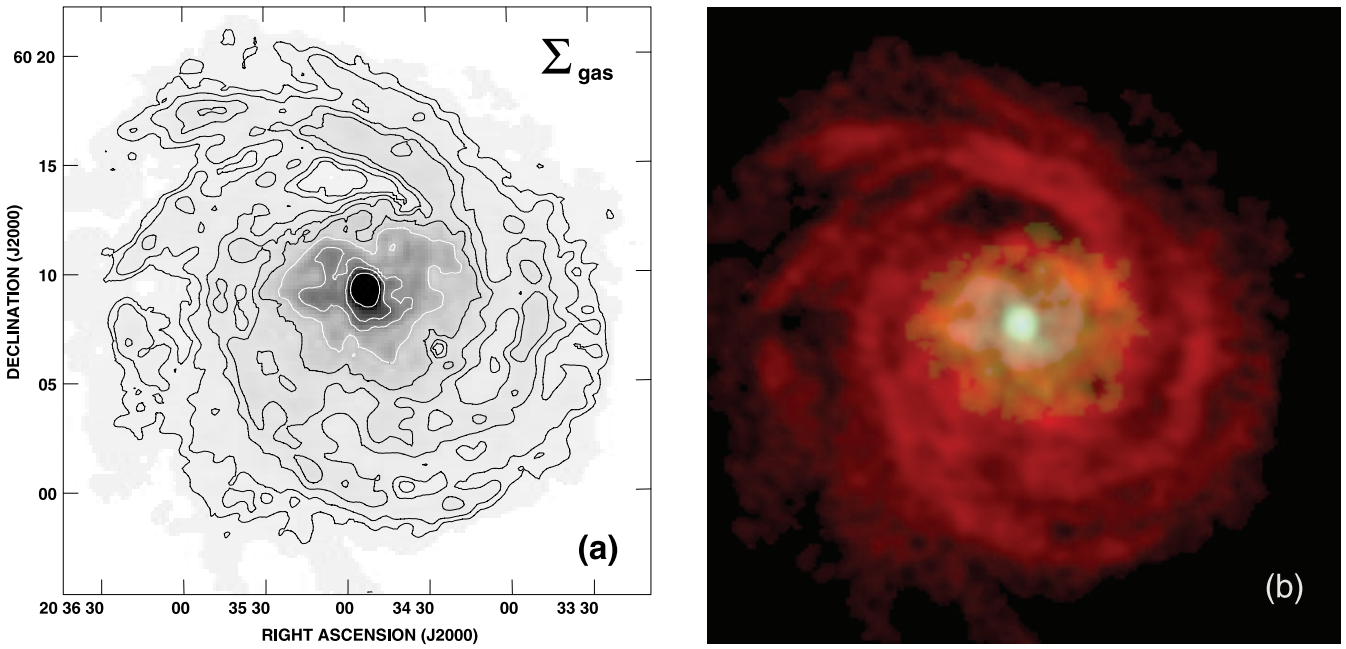

FIG. 9.—Neutral gas surface density in NGC 6946. (*a*) Map of the total neutral gas surface density, corrected for inclination (cos 40°) and increased by a factor of 1.36 for the He and heavier element content. This map does not include a missing H I flux estimate. Contours are at 1, 2, 4, 6, 10, 20, 40, 60, and 100 $M_\odot$ pc^{-2}. (*b*) False-color image with CO(1–0) in green and H I in red. Regions of nearly equivalent column densities show up in orange. The CO(2–1) emission has been added in blue to bring out the bright CO nucleus.

range of radii used by Tacconi & Young (1986) and Walsh et al. (2002): 40″–280″ and 60″–260″, respectively. We conclude that the CO falls off with an exponential scale length of $1.2' \pm 0.2'$ on arcminute scales when excluding the inner 1′ nuclear region, and of about 1′ if the nucleus is included.

A total neutral gas surface density map, $\Sigma_{\rm gas} = 1.36(\Sigma_{\rm H\,I} + \Sigma_{\rm H_2})$, is presented in Figure 9*a*. This map has been corrected for inclination but not for missing $\Sigma_{\rm H\,I}$ due to undersampling in the VLA image ($\sim$1 $M_\odot$ pc^{-2}). A false-color image is presented in Figure 9*b*, with H I in red and CO in green, so that the molecular contribution to the total gas disk can be distinguished. Values for $\Sigma_{\rm gas}$ range from 240 $M_\odot$ pc^{-2} at the nucleus, to 20–45 $M_\odot$ pc^{-2} along the spiral arms within the optical part of the galaxy, to 5–10 $M_\odot$ pc^{-2} for the outer arms. At first glance, H_2 and H I blend into a single global gas structure extending from the nucleus to the outer gas disk. A closer look reveals some subtleties. In the southern part of NGC 6946, the neutral density gradient is smooth and gradual. In the north, the gradient is much steeper, with the gas density falling to a level of 20 $M_\odot$ pc^{-2} in 90″ (2.6 kpc) to the north, into an interarm void, as compared to a 180″ fall to the same mass density in the south (this can also be seen in Fig. 7). This steeper falloff on the northern side of the central gas peak may be related to the more well-defined spiral arm to the north, and perhaps also to the prominent northeastern optical arm (Arp 1966).

The global properties of three late galaxies for which we have a similar data set, along with those of the Milky Way for reference, are listed in Table 2. IC 342, M83, and NGC 6946 all have gas disks that extend well beyond their optical diameters, and all three show some evidence for a bar. The $\Sigma^{\rm disk}_{\rm H_2}$ values for IC 342, NGC 6946, and M83 are all significantly higher than that of the Milky Way: a factor of 4 higher for IC 342 and NGC 6946, and a factor of 7 higher for M83. The NGC 6946 $\Sigma^{\rm disk}_{\rm H_2}$ value is similar to that of IC 342, while its $\Sigma^{\rm nuc}_{\rm H_2}$ is intermediate between IC 342 and M83. All four galaxies have similar relative proportions of H_2 and H I; global $M_{\rm H_2}/M_{\rm H\,I}$ values between 0.3 and 0.5 are also seen in the nearby galaxy, Maffei 2 (Mason & Wilson 2004).

TABLE 2
PROPERTIES OF THREE LATE-TYPE GALAXIES AND THE MILKY WAY

PROPERTY	GALAXY			
	IC 342[a]	NGC 6946	M83[b]	Milky Way
Hubble type	Scd	Scd	SBc	SBbc
Distance (Mpc)	3.3[c]	6	4	...
$D_{\rm H_2}$ (arcmin)[d]	20	11	11	...
$D_{\rm H_2}/D_{\rm H\,I}$	0.23	0.38	0.15	...
$D_{\rm H_2}/D_{25}$[e]	1.1	1.0	1.0	...
$M_{\rm dynamical}$ (10^{11} $M_\odot$)	1.8[f]	1.9	0.7	$\sim$3[g]
$M_{\rm H_2,\,total}$ (10^8 $M_\odot$)	16[h,i]	33	23[i]	25[j]
$M_{\rm H\,I,\,total}$ (10^8 $M_\odot$)[k]	57[h]	70	62	48[l]
$M_{\rm H_2}/M_{\rm H\,I}$	0.27	0.47	0.37	0.52
$M_{\rm gas}/M_{\rm dyn}$[m]	0.055	0.074	0.16	0.03
$\Sigma^{\rm nucleus}_{\rm H_2}$ ($M_\odot$ pc^{-2})[n]	140	170	220	400[o]
$\Sigma^{\rm disk}_{\rm H_2}$ ($M_\odot$ pc^{-2})[p]	11	13	23	3.4[q]

[a] Data from Crosthwaite et al. (2001).
[b] Data from Crosthwaite et al. (2002).
[c] Latest distance estimate based on Cepheid variables (Saha et al. 2002).
[d] Using the radius at which the azimuthal average $\Sigma_{\rm H_2} \sim 0.5$ $M_\odot$ pc^{-2}.
[e] D_{25} from the Second Reference Catalogue of Bright Galaxies (de Vaucouleurs et al. 1976).
[f] Dynamical mass from Brandt model using 3.3 Mpc adjusted from 2 Mpc.
[g] Within 20 kpc (Nikiforov et al. 2000) from rotation curve modeling.
[h] Adjusted to 3.3 Mpc distance from 2 Mpc.
[i] Rescaled to a 2.0×10^{20} K km s^{-1} conversion factor.
[j] Combes (1991).
[k] Includes VLA missing flux estimates.
[l] Kulkarni & Heiles (1987).
[m] Gas includes a factor of 1.36 for He and heavier elements.
[n] In 55′ beam centered on the nucleus.
[o] For $R < 400$ pc (Scoville & Sanders 1987).
[p] Mean $\Sigma_{\rm H_2}$ from observed CO disk excluding the nucleus.
[q] For 400 pc $< R <$ 14 kpc (Scoville & Sanders 1987).

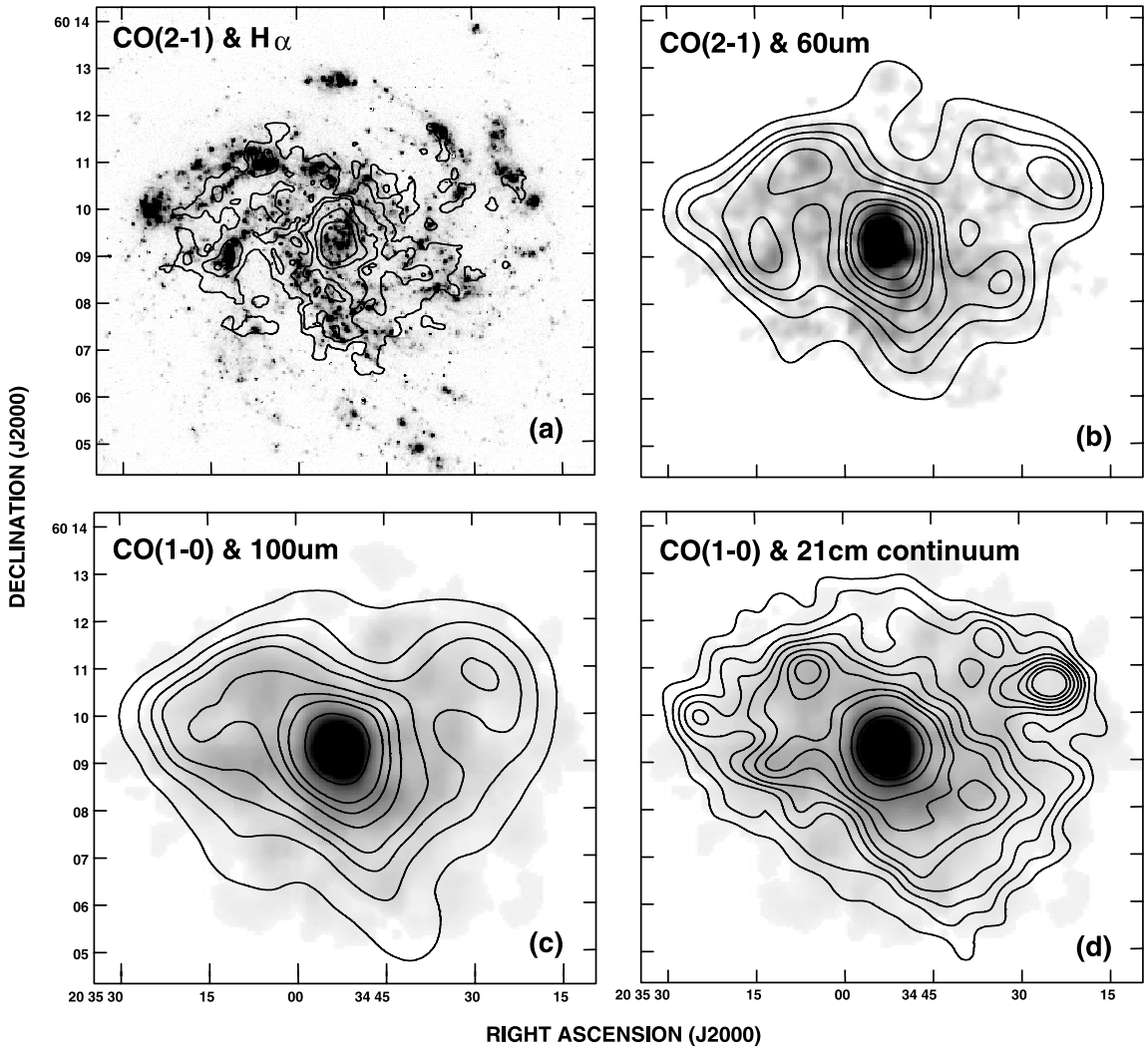

FIG. 10.—CO and star formation tracers in NGC 6946. The CO(1–0) and CO(2–1) beam sizes are 55″ and 27″, respectively. (*a*) I_{21} in contours and Hα in gray scale. The Hα image is from Ferguson et al. (1998) and is not presented here in calibrated units. The Hα image was regridded to 2″ pixels. The I_{21} contours are at 5, 10, 15, 30, and 50 K km s^{-1}. (*b*) I_{21} in gray scale with *IRAS* 60 μm contours. The gray scale ranges from 0 to 40 K km s^{-1}. The 60 μm contours are at 10, 20, 30, 40, 60, 90, 120, and 200 MJy sr^{-1}. The 60 μm beam size (FWHM) is 45″ × 41″, P.A. = 21°, and the rms noise level is 0.6 MJy sr^{-1}. (*c*) I_{10} in gray scale with *IRAS* 100 μm contours. The gray scale ranges from 0 to 40 K km s^{-1}. The 100 μm contours are at 20, 40, 60, 80, 120, 160, 200, and 300 MJy sr^{-1}. The 100 μm beam size (FWHM) is 69″ × 65″, P.A. = 20°, and the rms noise level is 2 MJy sr^{-1}. (*d*) I_{10} in gray scale with 21 cm continuum contours. The gray scale ranges from 0 to 40 K km s^{-1}. The 21 cm contours are at 5, 7, 10, 12, 18, 22, 25, 36, and 48 mJy beam^{-1}. The beam size (FWHM) is 49″ × 42″, P.A. = 73°, and the rms noise level is 1.2 mJy beam^{-1}.

M83 stands out as a particularly gas-rich object relative to its dynamical mass, with $M_{\rm gas}/M_{\rm dyn}$ a factor of 2 higher than for IC 342 and NGC 6946 and 4 times that of the Milky Way. The H_2 and optical disk diameters of the three external galaxies are the same, $D_{H_2}/D_{25} \sim 1$. The dynamical masses of these three galaxies are an order of magnitude smaller than that of the Milky Way, although their total gas mass is similar. It is difficult to place too much emphasis on the subtle variations that rely on distance estimates, since the uncertain distances to these nearby galaxies can easily affect their masses, both gaseous ($\propto R^2$) and dynamical ($\propto R$).

5. STAR FORMATION AND THE NEUTRAL GAS DISK OF NGC 6946

5.1. *Star Formation Tracers,* CO, *and the Neutral Gas Disk*

Because stars form from molecular gas, we expect to see correlations between CO and tracers of star formation. These tracers include Hα emission from ionized gas associated with massive young stars, FIR emission from dust heated by young stars, and radio continuum emission from relativistic electrons created by supernovae. To calculate linear correlation coefficients all the maps were convolved to the largest beam size in our collection of maps, a 70″ circular beam size, *then clipped to use* >3 σ *emission*, and sampled on a 35″ grid.

Hα emission (Ferguson et al. 1998) and I_{21} are compared in Figure 10*a*. The nuclear bar traced by Hα within the central 2′ is aligned with the elongation of the central I_{21} contours. The I_{21} arms are traced at higher resolution by the Hα emission. In the outer I_{21} disk, the brighter patches of CO(2–1) emission are aligned with the brightest patches of Hα, which is most clearly seen along the northeastern spiral arms. This supports the conjecture that the ring of H I emission seen at these radii is the result of photodissociated H_2. It is apparent from this map that the ratio of Hα emission to I_{21} is not the same in the nucleus and outer arms; due to substantial extinction, particularly in the nucleus, Hα is probably not the optimal tracer of star formation for this gas-rich galaxy. When Hα is compared to I_{21} or our primary molecular mass tracer, I_{10}, we obtain a linear correlation coefficient of ~0.65. The Hα correlations do not improve when

a 1′ diameter region centered on the nucleus is excluded from the correlation.

Figure 10*b* shows that the 60 μm FIR emission generally reproduces the morphology seen in I_{21} (*gray scale*), despite the noticeable artifacts (the "boxy" structure of the central contours) produced by the HiRes maximum entropy algorithm. An ISOPHOT 60 μm map by Tuffs et al. (1996) confirms the overall morphological structure seen in the HiRes map. The 60 μm nuclear peak is at $\alpha = 20^{\rm h}34^{\rm m}52.4^{\rm s}$, $\delta = 60^\circ 9' 15''$ (J2000.0), which is, within the uncertainties, coincident with the CO peak. If CO(2–1) along with 60 μm FIR trace a warmer component, both heated by star formation, we expect these emission pairs to have similar features in the disk. The 60 μm emission traces the overall CO(2–1) arm structure better than the 100 μm emission shown in Figure 10*c*. The four prominent peaks in the outer 60 μm emission disk are aligned with peaks in the outer I_{21} arm structure.

The 100 μm FIR and 21 cm continuum maps have resolution comparable to our CO map (Figs. 10*c* and 10*d*). The 100 μm emission roughly mimics the CO(1–0) emission disk, but the CO arm structure east of the nucleus is not well traced by the 100 μm emission. The 100 μm nuclear peak is at $\alpha = 20^{\rm h}34^{\rm m}53.0^{\rm s}$, $\delta = 60^\circ 9' 23''$ (J2000.0): northeast of the CO emission peaks. The radio continuum does a better job reproducing the CO morphology, with the exception of the 21 cm peak 4′ northwest of the nucleus. This is coincident with the suggestion that cosmic rays may be more important for the heating of molecular gas on large scales such as observed here than the radiation from in situ massive star formation (Adler et al. 1991; Suchkov et al. 1993). The continuum peak to the north and west of the nucleus at $\alpha = 20^{\rm h}34^{\rm m}24.9^{\rm s}$, $\delta = 60^\circ 10' 38''$ (J2000.0) is probably a background radio galaxy (based on its spectral index, $\alpha = -0.84$, and flux; van der Kruit et al. 1977). The 21 cm continuum nuclear peak at $\alpha = 20^{\rm h}34^{\rm m}52.4^{\rm s}$, $\delta = 60^\circ 9' 15''$ (J2000.0) is consistent with the CO(1–0) peak. Much of the outer CO arm morphology and prominent emission peaks are traced by nonthermal radio continuum.

Walsh et al. (2002) also found statistically significant correlations between CO(1–0) emission and the total radio continuum at 6 cm, and between CO(1–0) and 20 cm nonthermal continuum in NGC 6946. When fluxes are extrapolated to the expected 20 cm values (Condon 1992 using $S_\nu \propto \nu^{-0.8}$), we obtain a mean I_{10}/T_{20} of 1.4 ± 0.5 km s^{-1} from our 70″ beam convolved maps for the disk of NGC 6946. This is higher than the $I_{10}/T_{20} = 1.0$ value determined by Adler et al. (1991) from sparely sampled I_{10} data, but in line with the 1.3 mean value for all the galaxies in their sample.

One might naively think that the FIR has a more direct causal link to newly formed stars, while radio continuum emission, which arises from relativistic electrons produced in supernova remnants, would be more spatially removed. In reality the far-infrared cirrus and nonthermal disk emission on arcminute scales represent a less temporally localized reflection of star formation; the close correspondence of radio continuum and CO supports a model of cosmic-ray confinement on 1 kpc scale lengths, and highlights the importance of gas surface density in containing the magnetic field required to extract synchrotron emission from relativistic electrons (Bicay et al. 1989; Bicay & Helou 1990; Helou & Bicay 1993).

Table 3 lists least-squares fits to the radial distribution of ratios of I_{10} or I_{21} to our star formation tracers, $\rm gas_{tracer}/SF_{tracer}$. With the exception of Hα, all the star formation tracers are highly correlated with CO emission. From the 70″ beam maps we obtain linear correlation coefficients on the order of ~0.95 or better in comparisons between either of our CO maps and any of the star formation tracers except for Hα. The radial gradient is reduced by a factor of 2 when I_{10} is used instead of I_{21}, indicating that I_{10} remains the best tracer of molecular gas associated with star formation on kiloparsec scales.

TABLE 3

Radial Slope of Gas–to–Star Formation Tracer Ratios

Gas Tracer[a]	SF Tracer[a]	Slope[b]
I_{21}	100 μm	−0.196 (0.015)
I_{21}	60 μm	−0.189 (0.015)
I_{21}	21 cm continuum	−0.170 (0.014)
I_{21}	Hα	−0.224 (0.015)
I_{10}	100 μm	−0.102 (0.008)
I_{10}	60 μm	−0.095 (0.009)
I_{10}	21 cm continuum	−0.076 (0.009)
I_{10}	Hα	−0.130 (0.014)
$\Sigma_{\rm gas}$[c]	100 μm	−0.002 (0.006)
$\Sigma_{\rm gas}$	60 μm	0.005 (0.007)
$\Sigma_{\rm gas}$	21 cm continuum	0.024 (0.007)
$\Sigma_{\rm gas}$	Hα	−0.030 (0.013)

[a] Maps were convolved to a 70″ circular beam size and clipped at 3 σ. The region containing the bright 21 cm continuum emission, tentatively identified as a background galaxy, at $\alpha = 20^{\rm h}34^{\rm m}24.9^{\rm s}$, $\delta = 60^\circ 10' 38''$ (J2000.0) was clipped from all the comparison maps.

[b] Slope (ratio/arcminute) and rms uncertainty (in parentheses) from a least-squares fit to the ratio of gas tracer to formation tracer as a function of Galactic radius: $\log(\rm gas_{tracer}/SF_{tracer}) = Ar + B$. The maps were sampled on a grid of half–beam width points (35″).

[c] The molecular gas surface density derived from CO plus the atomic gas surface density derived from H I, increased by a factor of 1.36 to account for He and heavier elements.

While CO is highly correlated with star formation tracers, the correlation of total gas, H I+CO, is even better (see Table 3). The radial gradient is reduced by a factor of 10 when $\Sigma_{\rm gas}$ is used. If we assume that the 21 cm and FIR emission trace star formation, this result implies that the star formation rate (SFR) in NGC 6946 is more closely tied to $\Sigma_{\rm gas}$ than $\Sigma_{\rm H_2}$. Restating this result: a simple Schmidt law applies, SFE $\propto \Sigma_{\rm gas}^n$ (Schmidt 1959; Kennicutt 1998b), at least on kiloparsec scales. *Moreover, it appears that in the outer parts of NGC 6946, star formation is likely to take place in regions of predominantly* H I *gas*.

We obtained similar results for IC 342 and M83 (Crosthwaite et al. 2001, 2002). While the correlation coefficient for $\Sigma_{\rm gas}/S_{21\ \rm cm}$ in M83 is also high, 0.95, for IC 342 the correlation coefficient is only 0.73. The lower map correlation for IC 342 is related to the peculiar one-armed appearance of the 21 cm continuum map, which contrasts starkly with its grand-design appearance in other tracers. From least-squares fits to the $\Sigma_{\rm gas}/S_{21\ \rm cm}$ ratio we obtain slopes of -0.012 ± 0.004 (dex) for IC 342 and -0.13 ± 0.02 (dex) for M83. For M83 the slope is not as flat as in IC 342 and NGC 6946. This gradient in M83 may indicate an age difference, with larger $\Sigma_{\rm gas}/S_{21\ \rm cm}$ values resulting from younger star-forming regions in its disk (Suchkov et al. 1993). The $\Sigma_{\rm gas}/S_{21\ \rm cm}$ comparison for NGC 6946 suffers none of these peculiarities.

A complication in the interpretation of molecular gas mass could arise because of a radial gradient in metallicity and because the Galactic CO conversion factor overpredicts the H_2 mass in the nucleus of NGC 6946 (Meier & Turner 2004). Based on the metallicity gradient for NGC 6946 measured by Belley & Roy (1992) and the metallicity adjustment to the CO conversion factor used by Wilson (1995) for giant molecular clouds in M33, $X_{\rm CO}$ could be a factor of 2 higher at the edge of the NGC 6946 CO disk. This would increase the molecular surface density derived from CO at the disk edge by a factor of 2 and potentially reduce the radial gradient of molecular mass. However, this variation in

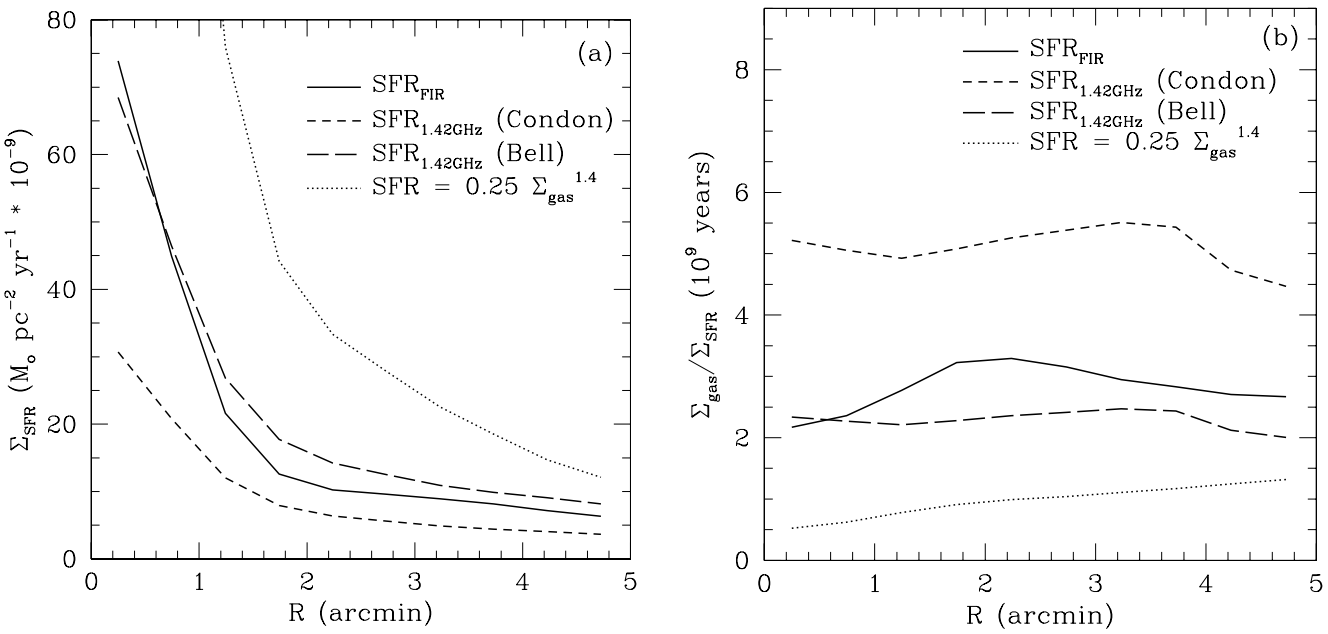

FIG. 11.—Radial SFRs and efficiencies in NGC 6946. (*a*) Σ_{SFR} derived from the *IRAS* luminosities, L_{FIR}; from nonthermal radio continuum luminosity, L_{ntc} using the SFR calibration of Condon (1992) and L_{ntc} using the SFR calibration of Bell (2003); and as predicted using the Schmidt law by Kennicutt (1998a) from Σ_{gas}. (*b*) SFE expressed in terms of τ_{SFE}, the time it would take to consume all of the molecular gas at the given SFR. The legends in both panels indicate the source of the SFR calibration. At our assumed distance of 6 Mpc, $1' = 1.75$ kpc.

X_{CO} does not appear to be universal in low-metallicity systems (Meier et al. 2002; Leroy et al. 2005), so we do not adopt the correction here.

5.2. *The Star Formation Efficiency of the Disk of NGC 6946*

Studies of the links between star formation and gas, or star formation efficiency (SFE), have recently focused on correlations as a function of position in the galaxy, as opposed to global measures. Rownd & Young (1999) examined the relation between Σ_{H_2} and the SFR as traced by Hα; Murgia et al. (2002) compare a radio-continuum-based SFR and Σ_{H_2}; Wong & Blitz (2002) compare a SFR from Hα emission to Σ_{gas}. Young & Scoville (1982) pointed out that the falloff of Σ_{H_2} in NGC 6946 with radius was very similar to the falloff in *B* luminosity, implying a constant SFR per unit H_2. The most widely used formulation is the Schmidt law, $\Sigma_{SFR} = A\Sigma_{gas}^N$ (Schmidt 1959), and the most widely accepted calibration was done by Kennicutt (1998a), who finds $A = (2.5 \pm 0.7) \times 10^{-4}$ and $N = 1.4 \pm 0.15$ for Σ_{gas} in $M_\odot$ pc^{-2} and Σ_{SFR} in $M_\odot$ yr^{-1} kpc^{-2}. How well does the Schmidt law describe star formation in NGC 6946?

We can estimate SFRs from our FIR and 21 cm continuum data. Unlike Hα emission, these tracers are relatively unaffected by absorption. Although cirrus heated by an older population of stars may contaminate FIR in some galaxies, this is probably not a big effect in Scd-type spirals (Sauvage & Thuan 1992). The 21 cm continuum appears to be a good star formation tracer on global scales, although it must break down at smaller scales. The maps for this analysis were convolved to the largest circular beam in the set, 70″.

We built a FIR map from the 60 and 100 μm *IRAS* maps using

$$S_{FIR}\left(\text{W m}^{-2}\text{ sr}^{-1}\right) = 12.6\times10^{-14} \times\left[2.58S_{60\,\mu m}\left(\text{Jy sr}^{-1}\right) + S_{100\,\mu m}\left(\text{Jy sr}^{-1}\right)\right]$$

(Lonsdale et al. 1985). We adopt the FIR SFR:

$$\text{SFR}_{FIR}\left(M_\odot\text{ yr}^{-1}\right) = 4.5\times10^{-37}L_{FIR}(\text{W})$$

(Kennicutt 1998b), where $L = 4\pi D^2 S$ and D is the distance to NGC 6946. We derive the $\Sigma_{SFR_{FIR}}$ map from the S_{FIR} map using

$$\Sigma_{SFR_{FIR}}\left(M_\odot\text{ yr}^{-1}\text{ pc}^{-2}\right) = 5.38\times10^{-3}S_{FIR}\left(\text{W m}^{-2}\text{ sr}^{-1}\right)\cos i,$$

where cos ($i = 40°$) gives us face-on surface values. For the nonthermal continuum at 21 cm we use

$$\text{SFR}_{ntc}\left(M_\odot\text{ yr}^{-1}\right) = 1.9\times10^{-22}\nu^{0.8}(\text{GHz})L_{ntc}\left(\text{W Hz}^{-1}\right)$$

to get the SFR (Condon 1992) and use

$$\Sigma_{SFR_{ntc}}\left(M_\odot\text{ yr}^{-1}\text{ pc}^{-2}\right) = 2.30\times10^{-7}S_{1.42\text{ GHz}}\left(\text{Jy beam}^{-1}\right)\cos i$$

to build the $\Sigma_{SFR_{ntc}}$ map. The Σ_{SFR} maps were azimuthally averaged in 30″ radius bins.

The results are shown in Figure 11*a*. The SFRs derived from the FIR and radio continuum differ by a factor of 2. Bell (2003) finds that the nonthermal continuum from low-luminosity galaxies is substantially suppressed, and so calibrations of the SFR from radio continuum from surveys that do not take into account the overall luminosities of the constituent galaxies tend to underestimate the SFR. Bell provides an alternate calibration:

$$\text{SFR}_{ntc}\left(M_\odot\text{ yr}^{-1}\right) = \frac{5.5\times10^{-22}}{0.1 + 0.9(L/L_c)^{0.3}}L_{ntc}\left(\text{W Hz}^{-1}\right),$$

where the total galactic flux satisfies the condition $L \le L_c$, $L_c = 6.4\times10^{21}$ W Hz^{-1}. In the case of NGC 6946, $L = 5.2\times10^{21}$ W Hz^{-1}. This calibration of SFR_{ntc} is also shown in Figure 11*a* and agrees with the FIR-derived rate. Although the agreement with the SFR_{FIR} result is clearly promising, this alternate calibration was established using total galaxy fluxes and has not been studied with respect to the varying nonthermal continuum fluxes within galaxies. Figure 11*a* also shows the SFR predicted by the Kennicutt (1998a)

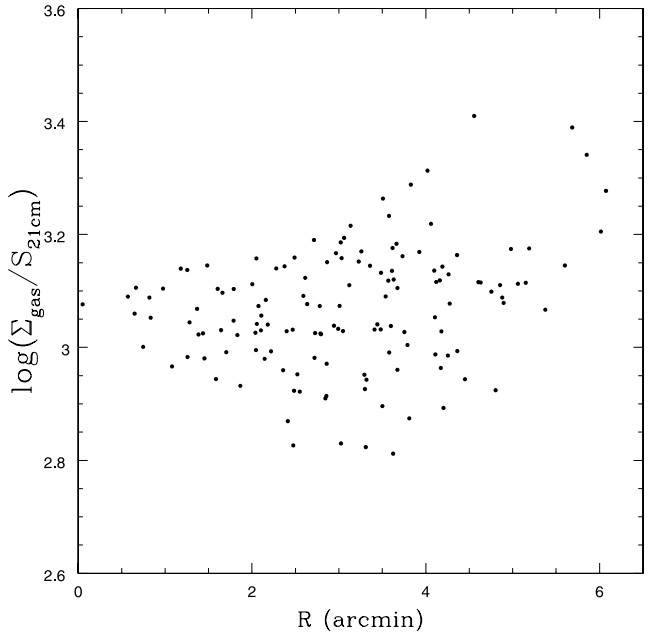

FIG. 12.—Ratio of total gas surface density to 21 cm continuum in NGC 6946. The gas surface density maps were convolved to a 70″ FWHM beam size and clipped at a 3 σ level prior to forming the ratios. The resulting ratio maps were sampled on a 35″ grid. At our assumed distance of 6 Mpc, $1' = 1.75$ kpc.

calibration of the Schmidt law using our Σ_{gas} map; in NGC 6946 it overestimates the SFR relative to the SFR_{FIR} and SFR_{ntc} values.

Another way to look at the Schmidt law is in terms of the SFE. In Figure 11*b* we express the SFE for each of our SFRs as τ_{SFE}, the time it would take to consume all the gas at the given SFR, $\tau_{SFE} = \Sigma_{SFR}/\Sigma_{gas}$. Using the SFR_{FIR} and Bell's calibration for SFR_{ntc}, the mean τ_{SFE} for NGC 6946 is 2.8 ± 0.8 Gyr, and $\Sigma_{SFR} \propto \Sigma_{gas}$. This is consistent with the mean τ_{SFE} of 2.6 Gyr for undisturbed galaxies found by Rownd & Young (1999). The $N = 1.4$ Schmidt law is also shown in Figure 11*b*; the Schmidt law overpredicts the SFE and its dependence on Σ_{gas}. Wong & Blitz (2002) found *N*-values as low as 1.1 for the galaxies in their sample. Elmegreen (2002; see references within) has noted that the Schmidt law is inconsistent with observations that the SFE is roughly constant across range of galactic environments. This certainly is the case for NGC 6946.

On kiloparsec scales the SFE for the nucleus of NGC 6946 does not differ from that of the disk; in other words, the strong central FIR emission from the nucleus of NGC 6946 results from having more molecular material from which to form stars rather than any increase in the SFE. This can be seen in Figure 12, where we show the radial distribution of the ratio of Σ_{gas} to 21 cm continuum; the ratio does not decline at the nucleus. The lowest values (highest efficiencies) are found between 2′ and 4′ radii (3.5–7 kpc). The highest values (lowest efficiencies) are at the largest radii. In two other late-type galaxies for which we have a similar data set, IC 342 and M83, there is a noticeable drop in $\log(\Sigma_{gas}/S_{21\,cm})$ from the peak values in the disk to the nucleus: an indication of an elevated SFE relative to the disk rates (Crosthwaite et al. 2001, 2002). Using the definition of Rownd & Young (1999) NGC 6946 would not be a starburst galaxy because it does not have a gas-cycling time shorter than 10^9 yr. Other authors have come to a similar conclusion about the SFE in NGC 6946: Meier & Turner (2004), based on a determination of the nuclear molecular mass from high-resolution observations of CO isotopes and multiple line transitions, and Madden et al. (1993), by evaluating the SFR using C II maps.

TABLE 4

COMPARISON OF THE MILKY WAY AND NGC 6946 AT LARGE *R*

	MILKY WAY[a,b]		NGC 6946[c]	
PROPERTY	8 kpc	12 kpc	8 kpc	12 kpc
$N_{H\,II}$ (kpc^{-2}).....	21	>1.4	~5[d]	~1[d]
Σ_{H_2} ($M_\odot$ pc^{-2}).....	2.9	>0.15	2.3 ± 1.7	...[e]
$\Sigma_{H\,I}$ ($M_\odot$ pc^{-2}).....	2.9	2.9	7–9[f]	3–5[f]

[a] Using $R_\odot = 8$ kpc.
[b] Values from the discussion in Wouterloot et al. (1988).
[c] Using a distance to NGC 6946 of 6 Mpc.
[d] The H II region positions from Hodge & Kennicutt (1983) were sampled on a grid of points separated by 10″. The points were regrouped into 20″ wide Galactic radius bins. The 12 kpc value was extrapolated from the resulting $N_{H\,II}$ (number per kpc^2) curve.
[e] Beyond our measured CO disk.
[f] Including the estimated flux missing from the VLA map would increase these by 1.2 $M_\odot$ pc^{-2}.

5.3. *Is There an Edge to the* CO *Disk in NGC 6946?*

Does the outer edge of our CO(1–0) map represent a real threshold for the formation of molecular clouds? Clearly, in NGC 6946 there is not a steep or marked decline in the gas as we detected in M83; that galaxy has a real gas edge, in both CO and H I, possibly due to tidal interaction (Crosthwaite et al. 2002). In NGC 6946 the exponential disk continues as far as we can detect it (Fig. 8). But there may be other subtle changes in the gas with radius, and we examine these below.

We use our Galaxy as a guide on what to expect for the radial falloff in gas and star formation in a spiral galaxy. The number of H II regions per kpc^2, Σ_{H_2}, and $\Sigma_{H\,I}$ at 1 $R_\odot$ and 12 kpc (rescaled to 1 $R_\odot = 8$ kpc) for the Milky Way from Wouterloot et al. (1988) are presented in Table 4. In the Galaxy, between 8 and 12 kpc $N_{H\,II}/1$ kpc^2 has fallen off by a factor of 15 and Σ_{H_2} by a factor of 20, while $\Sigma_{H\,I}$ stays relatively flat.[6] Star formation per unit H_2 remains relatively constant over this range of radii. Wouterloot et al. (1988) found evidence for molecular outflows at distances as large as 16 kpc. Lequeux et al. (1993) detected Galactic molecular gas in a search for CO absorption lines against continuum sources; their findings suggest cold molecular gas may be far more abundant at large radii than previously suspected. They suggest the molecular gas mass may be 4 times the H I mass at 12 kpc. Mead & Kutner (1988) detect a sparse distribution of Milky Way molecular clouds at 13 kpc with a mean $T_r^* \sim 3$ K and a mean radius of 20 pc.

The edge of the observed CO disk in NGC 6946 lies midway between 8 and 12 kpc for an assumed distance of 6 Mpc. Comparing NGC 6946 to the Milky Way (Table 4), at 8 kpc (4.6′) $N_{H\,II}/1$ kpc^2 is a factor of 4 less in NGC 6946 than the Galactic value at 1 $R_\odot$, and could be due to extinction in Hα, Σ_{H_2} is the same for both galaxies (within the errors), and $\Sigma_{H\,I}$ is at least twice the Galactic value. At 12 kpc, $N_{H\,II}/1$ kpc^2 is the same as Galactic (extrapolating 20″ in radius past the radial limit of the Hodge & Kennicutt [1983] data set), Σ_{H_2} is no longer detected in NGC 6946 by our observations, and $\Sigma_{H\,I}$ is at least as large as the value for the Milky Way. We conclude that given the similarity of $N_{H\,II}/1$ kpc^2 and $\Sigma_{H\,I}$ between these two galaxies, we would expect that Σ_{H_2} in NGC 6946 should be also be >0.1 $M_\odot$ pc^{-2} at 12 kpc.

[6] Caveat: these are not azimuthal averages but rather represent volumes at the Sun and a variety of viewing angles centered on a Galactic anticenter vector, and may not be representative of the Galaxy as a whole.

Complicating these comparisons is the uncertainty in the NGC 6946 distance. To date, there are no Cepheid-based distance estimates to NGC 6946, which has a low Galactic latitude. Recent estimates are (in megaparsecs) 5.7 ± 0.7 based on Type II SNe (Eastman et al. 1996), 6.4 ± 0.4 based on the brightest stars (Sharina et al. 1997), and 5.9 ± 0.4 based on blue supergiants (Karachentsev et al. 2000). As with any comparison based on absolute scales, our comparison changes if the 6 Mpc distance estimate is incorrect by more than ± 0.5 Mpc.

The mapping of the CO disk presented here is sensitivity-limited; our detection limit is 2–3 $M_\odot$ pc^{-2}. A combination of low T_{ex} and a low filling factor for molecular clouds in the beam combine to create a detection limit rather than a real threshold. There is also the possibility that declining metallicity in the outer disk lowers the CO emissivity relative to N_{H_2}, although this effect has yet to be seen. There are probably clouds here, but more widely dispersed than they are in the inner parts of the NGC 6946.

But our suspicion that there is substantial molecular gas at large galactic radii is not based entirely on a comparison to the Milky Way. There are theoretical reasons to expect molecular gas at radii beyond our detected CO edge (Elmegreen 1989, 1993; Elmegreen & Parravano 1994; Honma et al. 1995). According to Elmegreen & Parravano (1994), molecular clouds are not formed where the ISM pressure, P_{ISM}, becomes too low to facilitate the formation of cold, dense clouds. Or conversely, molecular clouds form in regions where $P_{ISM} > P_{min}$. The outer H I disk of NGC 6946 has considerable surface density structure that exists on kiloparsec in-plane size scales and where P_{ISM} may locally exceed this minimum. To calculate the midplane gas pressure we use

$$P_{ISM} = 0.5\pi G\Sigma_{gas}^2,$$

where we have ignored the stellar contribution to the pressure, which can only act to increase the value (Elmegreen & Parravano 1994). Along the outer ($R \sim 6'$, 10 kpc) H I gas arms, $P_{ISM} \sim 2 \times 10^3$ cm^{-3} K, which is close to P_{ISM} values at the edge of the CO disk. The outer gas arms are where one would expect to find molecular gas, if we had deeper maps. Several of the H II regions identified by Hodge & Kennicutt (1983) are located beyond the edge of our CO disk, particularly to the south, and it is likely that they are associated with molecular clouds that are too beam-diluted and cold to show up in our images. Ferguson et al. (1998) have detected Hα emission associated with the formation of massive stars, up to 3′ beyond our CO disk edge and precisely at the local maxima in the outer H I arms of NGC 6946. These star-forming outer arms would be good places to look for CO with a smaller beam and higher sensitivity.

Based on theoretical arguments and the detection of Hα in NGC 6946 at large galactic radii, the answer is: no, the "edge" of the CO disk at a galactocentric radius of 5′ (~9–10 kpc) in our images is not a real edge, it is a detection limit. There is no significant change in properties to indicate that the disk is undergoing a change at this radius. There could easily be molecular clouds that escape detection beyond this radius

6. CONCLUSIONS

We have obtained deep CO(1–0) and CO(2–1) images of a $10' \times 10'$ region centered on the Sc galaxy NGC 6946, with 55″ and 27″ resolution using the NRAO 12 m telescope. We have combined these deep CO images with VLA H I images to construct images of the neutral gas in this galaxy. To summarize our findings:

1. The CO(1–0) and CO(2–1) disks shows many of the same features seen in the optical disk: a strong nuclear peak of emission, molecular gas arms spatially coincident with the asymmetric optical arm pattern, and a 10′ diameter inner disk filled with CO emission. The CO disk is roughly exponential with a scale length of $1.2' \pm 0.2'$ or $(2 \pm 0.3)(D/6$ Mpc) kpc.

2. We obtain $(3.3 \times 10^9)(D/6$ Mpc$)^2$ $M_\odot$ for the molecular hydrogen gas mass of NGC 6946. This can be compared to the total atomic hydrogen gas mass of $M_{H\,I} = 7.0 \times 10^9 (D/6$ Mpc$)^2$ $M_\odot$ (which includes a VLA missing flux estimate). Molecular hydrogen constitutes one-third of the interstellar hydrogen gas mass and 2% of the dynamical mass of NGC 6946. At the nucleus, $\Sigma_{H_2} = 170$ $M_\odot$ pc^{-2}, and the molecular gas surface density is >20 $M_\odot$ pc^{-2} along the strong optical arm pattern and ~10 $M_\odot$ pc^{-2} in regions beyond.

3. The mean value for $r_{12} = I_{CO(2-1)}/I_{CO(1-0)}$ in the nucleus and optical arm pattern is $\sim 0.83 \pm 0.14$. This is consistent with optically thick gas, with an excitation temperature of 10–15 K. Interarm CO shows the largest variation in r_{12}, with a range of 0.35 to 2. Only 5% of the CO ratio map has $r_{12} < 0.6$, which is likely to be cold or subthermally excited CO ($T_{ex} < 4$ K). Fully half of the CO disk of NGC 6946 has $r_{12} > 1$. The high r_{12} appears to indicate the presence of widespread, optically thin gas in between the spiral arms.

4. Molecular gas dominates the total gas surface density within a galactocentric radius of 3.5′ (6 kpc). CO emission fills the central depression in the H I disk. Beyond the nuclear region, there is a good correlation between the CO and H I gas, which both peak on the spiral arms. The inner disk arm pattern transitions smoothly from predominantly CO arms to predominantly H I arms at the outskirts of the CO disk. At the nucleus, $\Sigma_{gas} = 240$ $M_\odot$ pc^{-2}, and the total gas surface density is >20–45 $M_\odot$ pc^{-2} along the optical arm pattern and ~5–10 $M_\odot$ pc^{-2} along the outer gas arms [$\Sigma_{gas} = 1.36(\Sigma_{H_2} + \Sigma_{H\,I})$]. CO(2–1) emission peaks are coincident with clumps of H I, Hα, and FIR emission outside the nuclear region, presumably an indication of warmer molecular gas and dissociated H_2.

5. We find strong correlations between star formation tracers (except for Hα) and CO emission in NGC 6946. The correlation coefficients are ~0.95. When Σ_{gas} is used instead of just the molecular gas tracer in a radial comparison, the dependence on galactic radius is reduced. Star formation is more closely related to the total gas surface density than the molecular gas surface density alone, a Schmidt-law relationship. This also implies star formation is likely well beyond the radial limits of our observed CO disk in regions of predominantly H I gas. Surprisingly, Hα is not as well correlated with CO or Σ_{gas} as are the other star formation tracers. The correlation coefficient is significantly less, ~0.65, and the ratio formed from Hα and CO or Σ_{gas} declines more rapidly with galactic radius.

6. The SFE in the disk of NGC 6946 is relatively uniform: 2.8 Gyr when expressed in terms of the gas consumption timescale. This uniformity implies $\Sigma_{SFR} \propto \Sigma_{gas}$. The SFR at the nucleus is due to the high molecular surface density rather than an elevated SFE.

7. The edge of the observed CO disk represents a detection limit rather than a threshold for molecular cloud formation. We suspect the exponential fall of the CO disk continues smoothly past our detection limit. The midplane gas pressure in the outer H I arm structure, $P_{ISM} \sim 2 \times 10^3$ cm^{-3} K, is close to the value at the limits of the observed CO disk. These gas arms should support the formation of molecular clouds, which could be detectable in higher resolution observations.

The authors would like to thank the NRAO 12 m telescope operators, Duane Clark, Paul Hart, Victor Gasho, and Harry Stahl, for their help and company during the many observing sessions in

which the data for NGC 6946 and other galaxies were acquired. We thank L. Tacconi giving for us permission to retrieve and use the H I 21 cm line observations from the VLA archive, and we appreciate the careful reading and critical suggestions made by the anonymous referee. This work was supported in part by NSF grants AST 00-71276 and AST 03-07950. We made use of the NASA/IPAC/*IRAS* HiRes data reduction facilities, as well as STScI Digitized Sky Survey facilities. The Digitized Sky Surveys were produced at the Space Telescope Science Institute under US government grant NAG W-2166.

REFERENCES

Adler, D. S., Allen, R. J., & Lo, K. Y. 1991, ApJ, 382, 475
Arp, H. 1966, ApJS, 14, 1
Ball, R., Sargent, A. I., Scoville, N. Z., Lo, K. Y., & Scott, S. L. 1985, ApJ, 298, L21
Bell, E. F. 2003, ApJ, 586, 794
Belley, J., & Roy, J. 1992, ApJS, 78, 61
Bicay, M. D., & Helou, G. 1990, ApJ, 362, 59
Bicay, M. D., Helou, G., & Condon, J. J. 1989, ApJ, 338, L53
Boulanger, F., & Viallefond, F. 1992, A&A, 266, 37
Carignan, C., Charbonneau, P., Boulanger, F., & Viallefond, F. 1990, A&A, 234, 43
Casoli, F., Clausset, F., Combes, F., Viallefond, F., & Boulanger, F. 1990, A&A, 233, 357
Castets, A., Duvert, G., Dutrey, A., Bally, J., Langer, W. D., & Wilson, R. W. 1990, A&A, 234, 469
Combes, F. 1991, ARA&A, 29, 195
Condon, J. J. 1992, ARA&A, 30, 575
Crosthwaite, L. P., Turner, J. L., Buchholz, L., Ho, P. T. P., & Martin, R. N. 2002, AJ, 123, 1892
Crosthwaite, L. P., Turner, J. L., Hurt, R. L., Levine, D. A., Martin, R. N., & Ho, P. T. P. 2001, AJ, 122, 797
Dahmen, G., Huttemeister, S., Wilson, T. L., & Mauersberger, R. 1998, A&A, 331, 959
DeGioia-Eastwood, K., Grasdalen, G. L., Strom, S. E., & Strom, K. M. 1984, ApJ, 278, 564
de Vaucouleurs, G., de Vaucouleurs, A., & Corwin, H. 1976, Second Reference Catalogue of Bright Galaxies (Austin: Univ. Texas Press)
Dickman, R. L., Snell, R. L., & Schloerb, F. P. 1986, ApJ, 309, 326
Eastman, R. G., Schmidt, B. P., & Kirshner, R. 1996, ApJ, 466, 911
Elmegreen, B. G. 1989, ApJ, 338, 178
———. 1993, ApJ, 411, 170
———. 2002, ApJ, 577, 206
Elmegreen, B. G., & Parravano, A. 1994, ApJ, 435, L121
Engargiola, G. 1991, ApJS, 76, 875
Ferguson, A. M. N., Wyse, R. F. G., Gallagher, J. S., & Hunter, D. A. 1998, ApJ, 506, L19
Gordon, K. J., Remage, N. H., & Roberts, M. S. 1968, ApJ, 154, 845
Helou, G., & Bicay, M. D. 1993, ApJ, 415, 93
Hodge, P. W., & Kennicutt, R. C., Jr. 1983, AJ, 88, 296
Honma, M., Sofue, Y., & Arimoto, N. 1995, A&A, 304, 1
Hunter, S. D., et al. 1997, ApJ, 481, 205
Ishizuki, S., Kawabe, R., Ishiguro, M., Okumura, S. K., Morita, K.-I., Chikada, Y., Kasuga, T., & Doi, M. 1990, ApJ, 355, 436
Kamphuis, J., & Sancisi, R. 1993, A&A, 273, L31
Karachentsev, I. D., Sharina, M. E., & Hutchmeier, W. K. 2000, A&A, 362, 544
Kennicutt, R. C., Jr. 1998a, ApJ, 498, 541
———. 1998b, ARA&A, 36, 189
Kulkarni, S. R., & Heiles, C. 1987, in Interstellar Processes, ed. D. Hollenbach & H. A. Thronson (Dordrecht: Reidel), 87
Kutner, M. L., & Ulich, B. L. 1981, ApJ, 250, 341
Lacey, C., Duric, N., & Goss, W. M. 1997, ApJS, 109, 417
Lequeux, J., Allen, R. J., & Guilloteau, S. 1993, A&A, 280, L23
Leroy, A., et al. 2005, ApJ, 625, 763
Lonsdale, C. J., et al., eds. 1985, Catalogued Galaxies and Quasars in the *IRAS* Survey (Pasadena: JPL)
Madden, S. C., Geis, N., Genzel, R., Herrmann, F., Jackson, J., Poglitsch, A., Stacey, G. J., & Townes, C. H. 1993, ApJ, 407, 579
Maloney, P., & Black, J. H. 1988, ApJ, 325, 389
Mangum, J. G. 1996a, On The Fly Observing at the 12 m (Green Bank: NRAO)
———. 1996b, User's Manual for the NRAO 12 m Millimeter-Wave Telescope (Green Bank: NRAO)
———. 1997, Equipment and Calibration Status for the NRAO 12 m Telescope (Green Bank: NRAO)
Mason, A. M., & Wilson, C. D. 2004, ApJ, 612, 860
Mead, K. N., & Kutner, M. L. 1988, ApJ, 330, 399
Meier, D. S., & Turner, J. L. 2001, ApJ, 551, 687
———. 2004, AJ, 127, 2069
Meier, D. S., Turner, J. L., & Beck, S. C. 2002, AJ, 124, 877
Morris, M., & Lo, K. Y. 1978, ApJ, 223, 803
Murgia, M., et al. 2002, A&A, 385, 412
Nikiforov, I. I., Petrovskaya, I. V., & Ninkovic, S. 2000, in IAU Colloq. 174, Small Galaxy Groups, ed. M. J. Valtonen & C. Flynn (ASP Conf. Ser. 209; San Francisco: ASP), 399
Oka, T., Hasegawa, T., Handa, T., Hayashi, M., & Sakamoto, S. 1996, ApJ, 460, 334
Oka, T., Hasegawa, T., Hayashi, M., Handa, T., & Sakamoto, S. 1998, ApJ, 493, 730
Pisano, D. J., & Wilcots, E. M. 2000, MNRAS, 319, 821
Regan, M. W., Thornley, M. D., Helfer, T. T., Sheth, K., Wong, T., Vogel, S. N., Blitz, L., & Bock, D. C.-J. 2001, ApJ, 561, 218
Regan, M. W., & Vogel, S. N. 1995, ApJ, 452, L21
Rogstad, D. H., Shostak, G. S., & Rots, A. H. 1973, A&A, 22, 111
Rownd, B. K., & Young, J. S. 1999, AJ, 118, 670
Saha, A., Claver, J., & Hoessel, J. G. 2002, AJ, 124, 839
Sakamoto, S. 1996, ApJ, 462, 215
Sakamoto, S., Hasegawa, T., Handa, T., Hayashi, M., & Oka, T. 1997, ApJ, 486, 276
Sakamoto, S., Hasegawa, T., Hayashi, M., Handa, T., & Oka, T. 1995, ApJS, 100, 125
Sakamoto, S., Okumura, S. K., Ishizuki, S., & Scoville, N. Z. 1999, ApJS, 124, 403
Sauvage, M., & Thuan, T. X. 1992, ApJ, 396, L69
Schlegel, E. M. 1994, ApJ, 434, 523
Schmidt, M. 1959, ApJ, 129, 243
Scoville, N. Z., & Sanders, D. B. 1987, in Interstellar Processes, ed. D. Hollenbach & H. A. Thronson (Dordrecht: Reidel), 21
Scoville, N. Z., Yun, M. S., Sanders, D. B., Clemens, D. P., & Waller, W. H. 1987, ApJS, 63, 821
Sharina, M. E., Karachentsev, I. D., & Tikhonov, N. A. 1997, Astron. Lett., 23, 373
Sofue, Y., Doi, M., Ishizuki, S., Nakai, N., & Handa, T. 1988, PASJ, 40, 511
Solomon, P. M., Rivolo, A. R., Barrett, J., & Yahil, A. 1987, ApJ, 319, 730
Spaans, M., Tielens, A. G. G. M., van Dishoeck, E. F., & Bakes, E. L. O. 1994, ApJ, 437, 270
Strong, A. W., et al. 1988, A&A, 207, 1
Suchkov, A., Allen, R. J., & Heckman, T. M. 1993, ApJ, 413, 542
Tacconi, L. J., & Young, J. S. 1986, ApJ, 308, 600
———. 1989, ApJS, 71, 455
———. 1990, ApJ, 352, 595
Tilanus, R. P. J., & Allen, R. J. 1989, ApJ, 339, L57
———. 1993, A&A, 274, 707
Tuffs, R. J., et al. 1996, A&A, 315, L149
Ulich, B. L., & Haas, R. W. 1976, ApJS, 30, 247
van der Kruit, P. C., Allen, R. J., & Rots, A. H. 1977, A&A, 55, 421
Wall, W. F., Jaffe, D. T., Bash, F. N., Israel, F. P., Maloney, P. R., & Baas, F. 1993, ApJ, 414, 98
Walsh, W., Beck, R., Thuma, G., Weiss, A., Wielebinski, R., & Dumke, M. 2002, A&A, 388, 7
Weliachew, L., Casoli, F., & Combes, F. 1988, A&A, 199, 29
Wiklind, T., Rydbeck, G., Hjalmarson, A., & Bergman, P. 1990, A&A, 232, L11
Wilson, C. D. 1995, ApJ, 448, L97
Wilson, C. D., & Scoville, N. 1991, ApJ, 370, 184
Wong, T., & Blitz, L. 2002, ApJ, 569, 157
Wouterloot, J. G. A., Brand, J., & Henkel, C. 1988, A&A, 191, 323
Young, J. S., & Scoville, N. Z. 1982, ApJ, 258, 467
———. 1991, ARA&A, 29, 581
Young, J. S., et al. 1995, ApJS, 98, 219